2003-03

Design and testing of a combustor for a turbo-ramjet for UAV and missile applications

Piper, Ross H.

Monterey, California. Naval Postgraduate School

NAVAL POSTGRADUATE SCHOOL
Monterey, California

THESIS

DESIGN AND TESTING OF A COMBUSTOR FOR A TURBO-RAMJET FOR UAV AND MISSILE APPLICATIONS

by

Ross H. Piper III

March 2003

Thesis Advisor: Garth V. Hobson
Second Reader: Raymond P. Shreeve

Approved for public release; distribution is unlimited

THIS PAGE IS INTENTIONALLY LEFT BLANK

REPORT DOCUMENTATION PAGE			Form Approved OMB No. 0704-0188
Public reporting burden for this collection of information is estimated to average 1 hour per response, including the time for reviewing instruction, searching existing data sources, gathering and maintaining the data needed, and completing and reviewing the collection of information. Send comments regarding this burden estimate or any other aspect of this collection of information, including suggestions for reducing this burden, to Washington headquarters Services, Directorate for Information Operations and Reports, 1215 Jefferson Davis Highway, Suite 1204, Arlington, VA 22202-4302, and to the Office of Management and Budget, Paperwork Reduction Project (0704-0188) Washington DC 20503.			
1. AGENCY USE ONLY *(Leave blank)*	**2. REPORT DATE** March 2003	**3. REPORT TYPE AND DATES COVERED** Master's Thesis	
4. TITLE AND SUBTITLE: Design and Testing of a Combustor for a Turbo-ramjet Engine for UAV and Missile Applications			**5. FUNDING NUMBERS**
6. AUTHOR(S) Ross H. Piper III			
7. PERFORMING ORGANIZATION NAME(S) AND ADDRESS(ES) Naval Postgraduate School Monterey, CA 93943-5000			**8. PERFORMING ORGANIZATION REPORT NUMBER**
9. SPONSORING / MONITORING AGENCY NAME(S) AND ADDRESS(ES) N/A			**10. SPONSORING / MONITORING AGENCY REPORT NUMBER**
11. SUPPLEMENTARY NOTES The views expressed in this thesis are those of the author and do not reflect the official policy or position of the Department of Defense or the U.S. Government.			
12a. DISTRIBUTION / AVAILABILITY STATEMENT Approved for public release; distribution is unlimited			**12b. DISTRIBUTION CODE**

13. ABSTRACT ***(maximum 200 words)***

An existing freejet facility was upgraded and its range of operation extended into the high subsonic regime for operation as a test rig for the development of a combined-cycle, turbo-ramjet engine. A combustor was designed, developed, and tested as the afterburner for the turbo-ramjet engine. At subsonic speeds with the afterburner running, an increase in thrust of 40% was measured over the baseline turbojet running at 80% spool speed. A Computational Fluid Dynamics model of the flow through the shrouded turbojet engine was developed and successfully used to assist in predicting the bypass ratio of the engine at different Mach numbers. Numerous recommendations were made to improve the operation of the test rig, to improve the performance of the turbo-ramjet engine, and refine the numerical models. These recommended improvements will extend the present capabilities to design and analyze small combined cycle engines which have an application in unmanned aerial vehicles and missiles.

14. SUBJECT TERMS turbo-ramjet, afterburner, UAV propulsion, missile propulsion, Computational Fluid Dynamics, OVERFLOW, freejet, small-scale engines			**15. NUMBER OF PAGES** 97
			16. PRICE CODE
17. SECURITY CLASSIFICATION OF REPORT Unclassified	**18. SECURITY CLASSIFICATION OF THIS PAGE** Unclassified	**19. SECURITY CLASSIFICATION OF ABSTRACT** Unclassified	**20. LIMITATION OF ABSTRACT** UL

THIS PAGE IS INTENTIONALLY LEFT BLANK

Approved for public release; distribution is unlimited

DESIGN AND TESTING OF A COMBUSTOR FOR A TURBO-RAMJET FOR UAV AND MISSILE APPLICATIONS

Ross H. Piper III
Lieutenant, United States Navy
B.S., United States Naval Academy, 1995

Submitted in partial fulfillment of the
requirements for the degree of

MASTER OF SCIENCE IN AERONAUTICAL ENGINEERING

from the

NAVAL POSTGRADAUTE SCHOOL
March 2003

Author: Ross H. Piper III

Approved by: Garth V. Hobson
Thesis Advisor

Raymond P. Shreeve
Second Reader

Max F. Platzer
Chairman, Department of Aeronautics

THIS PAGE IS INTENTIONALLY LEFT BLANK

ABSTRACT

An existing freejet facility was upgraded and its range of operation extended into the high subsonic regime for operation as a test rig for the development of a combined-cycle, turbo-ramjet engine. A combustor was designed, developed, and tested as the afterburner for the turbo-ramjet engine. At subsonic speeds with the afterburner running, an increase in thrust of 40% was measured over the baseline turbojet running at 80% spool speed. A Computational Fluid Dynamics model of the flow through the shrouded turbojet engine was developed and successfully used to assist in predicting the bypass ratio of the engine at different Mach numbers. Numerous recommendations were made to improve the operation of the test rig, to improve the performance of the turbo-ramjet engine, and refine the numerical models. These recommended improvements will extend the present capabilities to design and analyze small combined cycle engines which have an application in unmanned aerial vehicles and missiles.

THIS PAGE IS INTENTIONALLY LEFT BLANK

TABLE OF CONTENTS

LIST OF FIGURES

LIST OF TABLES

THIS PAGE IS INTENTIONALLY LEFT BLANK

I. INTRODUCTION

There have been many advances in air-breathing propulsion since the invention of the first gas turbine engine over sixty years ago. Single-cycle, airbreathing engines have been optimized to operate efficiently over a relatively narrow Mach number range as shown in Figure 1 below. The specific fuel consumption (SFC) of a high bypass turbofan is a minimum at subsonic speeds, a low bypass turbofan (usually with reheat) is optimized in the supersonic range below Mach 2, and the afterburning turbojet operates most efficiently in the Mach 3 to 4 range. Beyond Mach 4 the ramjet theoretically is the most efficient engine up to a Mach number of 6, beyond which the supersonic combustion ramjet (SCRAMjet) has been predicted to be most efficient at approximately Mach 8. The most striking feature of each of the engines shown in Figure 1 is that with increasing Mach number, the turbomachinery within each engine is reduced or completely eliminated.

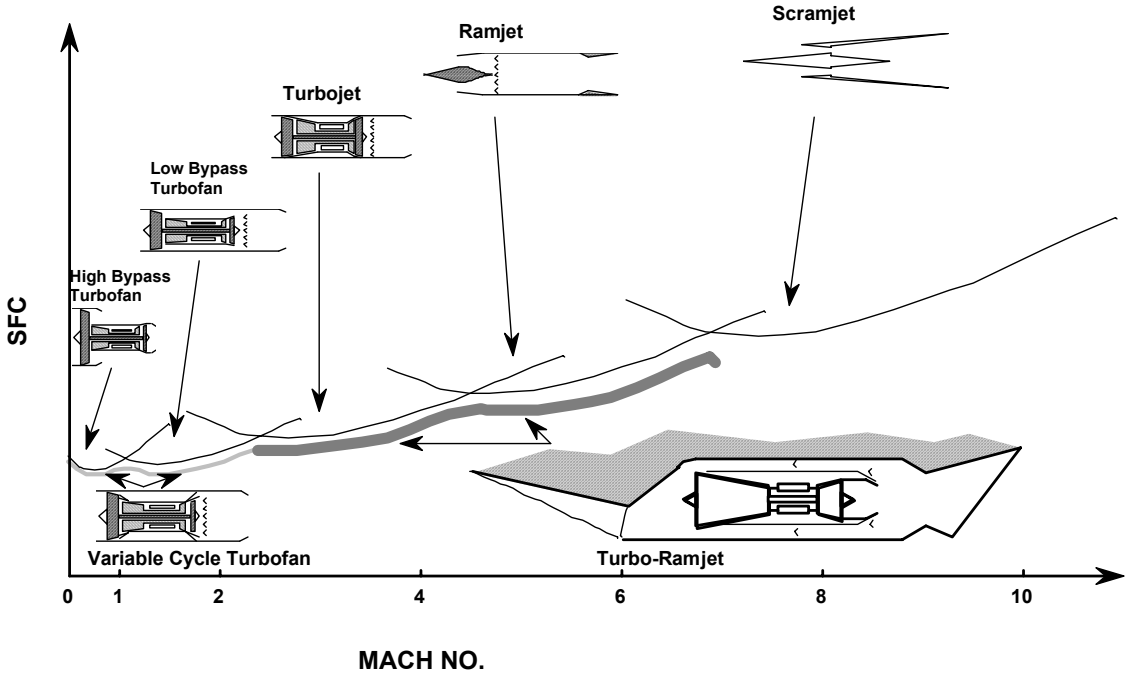

Figure 1. SFC vs. Mach Number for Airbreathing Engines

The only way to increase the operating range of airbreathing engines is to consider combined cycle engines (CCE), such as variable cycle turbofans for transonic flight and turbo-ramjet engines for high supersonic flight.

The first turbo-ramjet engine powered the Nord-Aviation Griffon II in 1953. The French Griffon II aircraft was a ramjet wrapped around a SNECMA Atar 101 E3 dry turbojet. By controlling the fuel flow rate to the two engines, the fraction of the total thrust generated by the ramjet varied from 0 under static conditions to over 80 percent at a flight Mach number of 2. It flew at Mach 2.1 at an altitude of 18,600 m (61,000 ft), and established a world speed record for the 100 km closed circuit of 1640 km/h in 1959 (Ref 1). In the early 1960's the United States developed the SR-71 Blackbird, which had two Pratt and Whitney J58 turbo-ramjet engines each producing 32,500 lbs thrust. It was capable of a cruise Mach number of 3.0 at an altitude of 24,400 m. In September 1974 one flew from New York to London in less than 2 hours, at an average speed of more than 2,900 km/h (1,800 mi/h). Maximum range at that speed was 4,825 km (3,000 mi) (Ref 2). Since the design of the SR-71 Blackbird the focus of research and testing has been limited to below Mach 3 or above Mach 6.

Despite the emphasis on the design and development of Unmanned Aerial Vehicles (UAVs) or Unmanned Combat Aerial Vehicles (UCAVs), there has been little published work with small-scale gas turbine engines. Most of these vehicles are designed and operated in the subsonic region using internal-combustion, propeller-driven engines or turbofan engines. The development of a small scale Combined Cycle Engine (CCE) that could self-sufficiently accelerate from rest to Mach 6 would clearly be a beneficial technology for high speed UAVs or UCAVs. In addition, a low cost self-sustaining turbo-ramjet would allow for UAVs half the size of those currently in operation to fly supersonically to targets, either to deliver ordinance or gather intelligence.

Work was started at the Naval Postgraduate School's Turbopropulsion Laboratory (TPL) in June 1998 to design and develop a turbo-ramjet engine. Initially, Rivera (Ref 3) tested the performance of the Sophia J450 engine, a low-cost turbojet engine for model aircraft. In March 1999, Hackaday (Ref 4) performed a study of the static performance

of the J450 with a constant area ejector. In September 1999, Andreou (Ref 5) tested the J450 in a shrouded duct of varying lengths with an elliptical intake.

In June 2000, al-Namani (Ref 6) continued the testing of the J450 in a shrouded duct of varying lengths. He measured engine shaft rotational speed and exhaust gas temperature on a remotely controlled and instrumented engine. Finally, he designed the current supersonic intake for a flight Mach number of 2.0.

In December 2000, Garcia (Ref 7) tested the ducted engine in a newly designed and constructed freejet facility at TPL. Tests were completed of the engine running with elliptical and supersonic intakes. He also tested the shrouded engine in the freejet facility at speeds less than Mach 0.5 with and without the engine running at various Mach numbers and engine spool speeds. Garcia used Computational Fluid Dynamics (CFD) to analyze the Mach number and pressure distributions of the shrouded engine intake at Mach 2. Finally, Garcia also completed preliminary design and testing for a fuel injection system (spray bars) for a possible afterburner/turbo-ramjet configuration.

The objective of this thesis was the design, development, and testing of a combustor or afterburner for the turbo-ramjet engine. It had to successfully light off under static conditions and remain operational with increasing forward speed. Experimental and computational tools were also developed for the analysis of such a combined cycle engine, which was also analyzed with currently available performance prediction software for conventional engines.

THIS PAGE IS INTENTIONALLY LEFT BLANK

II. ENGINE DEVELOPMENT PROGRAMS

A. EXPERIMENTAL SETUP

1. Overview

The purpose of this thesis was to design, develop, and test a combustor for a turbo-ramjet engine using the Sophia J450 jet engine as the gas generator. The J450 is a small commercially available turbojet engine that is in design and principle of operation very similar to a full-scale turbojet engine. Pertinent performance specifications are listed in Appendix A as Table A1.

2. Engine Test Rig

Figure 2 shows a schematic of the turbo-ramjet engine in the freejet facility as tested during the current research. Numerous modifications were implemented to facilitate development and testing of the turbo-ramjet. The original engine test rig was documented by Garcia in Ref 7. An additional strain-gauged thrust beam was added to the existing thrust stand. The additional beam increased the stiffness of the structure and provided for redundancy in measurement. An additional full Whetstone bridge was placed on the additional beam. The strain measuring systems from both beams were wired in parallel on the same data acquisition line. A concern that arose from prior testing was that the Angle of Attack of the engine changed with respect to Mach number as it pitched as a result of the large pressure forces. By securing the engine assembly with two thrust beams, the engine would remain horizontal at all Mach numbers.

At Mach numbers greater than 0.3, the forces on the engine were large enough to induce a transverse oscillatory condition. In order to reduce these oscillations and maintain stability, support bars were placed on each side of the engine assembly next to the forward engine mounting strut as shown in Figure 3. This eliminated the undesired vibrations and oscillations.

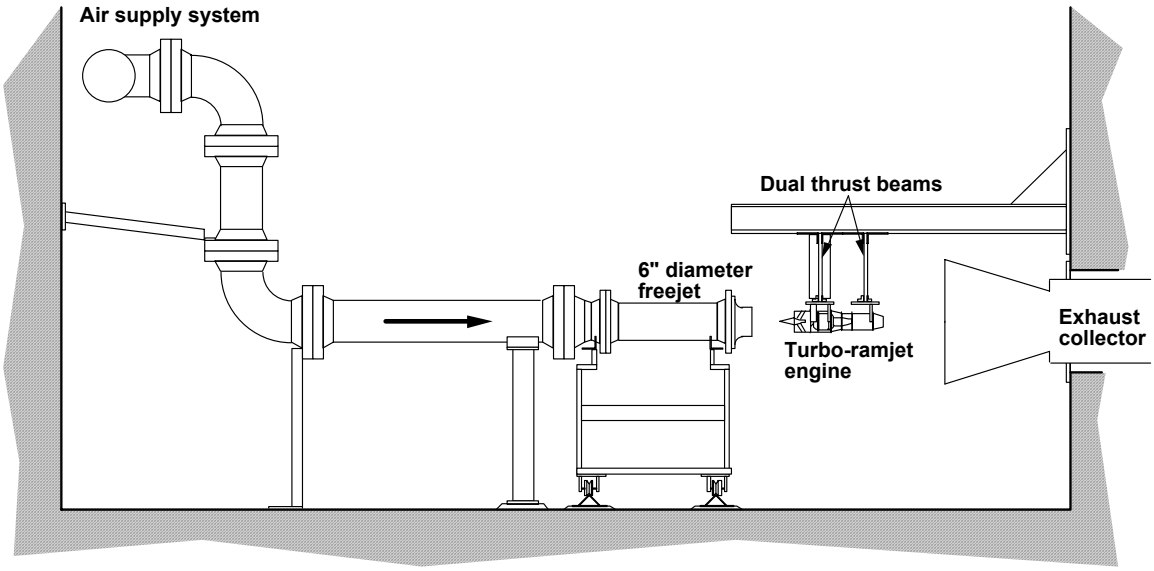

Figure 2. Schematic of Freejet Test Facility with Turbo-Ramjet Engine

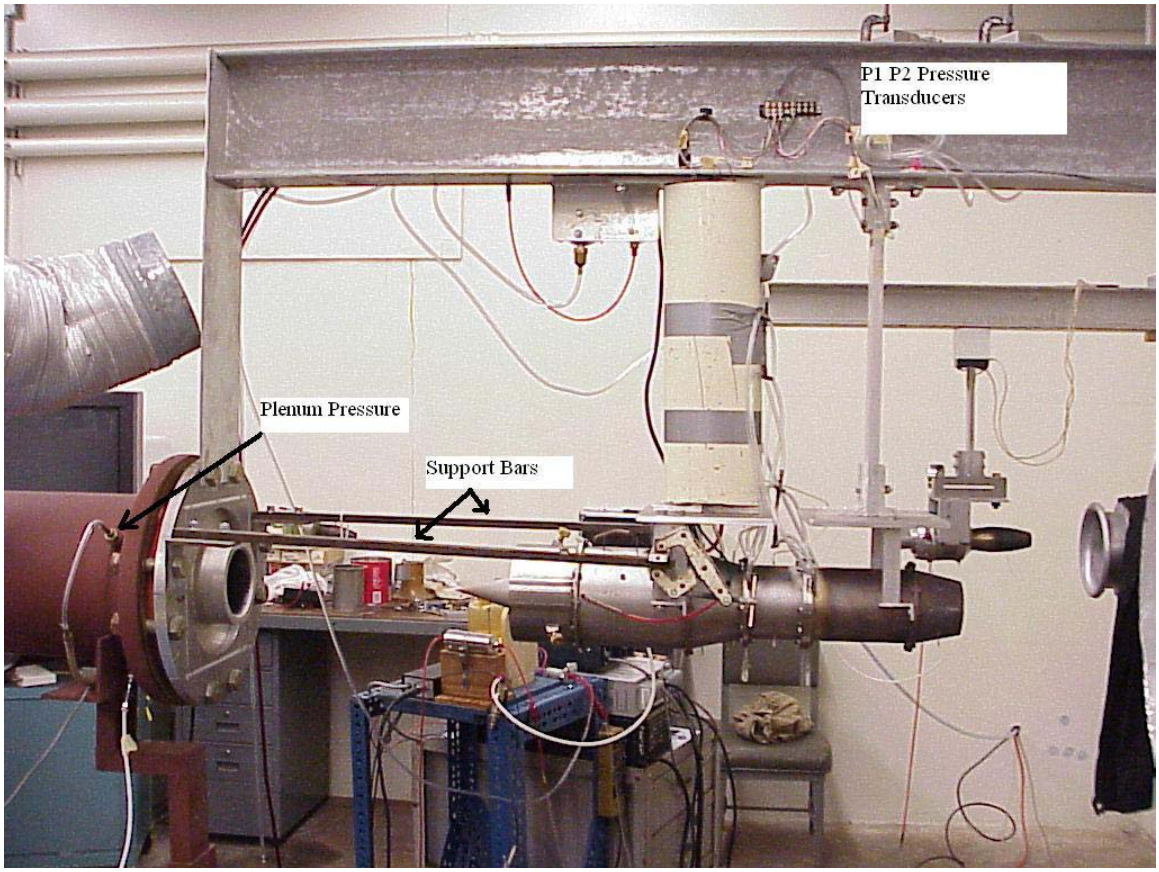

Figure 3. Engine Test Rig

One pressure transducer was installed on the freejet plenum upstream of the final 6" nozzle. Pressure transducers were mounted on the main I-beam to allow for pressure measurements throughout the length of the turbo-ramjet. Multiple video cameras were used as flow visualization tools and to document testing. A low pressure propane fuel system was installed for the ramjet combustor pilot light. An additional Coleman Fuel tank and delivery system were installed to provide fuel to the ramjet combustor as shown in Figure 4.

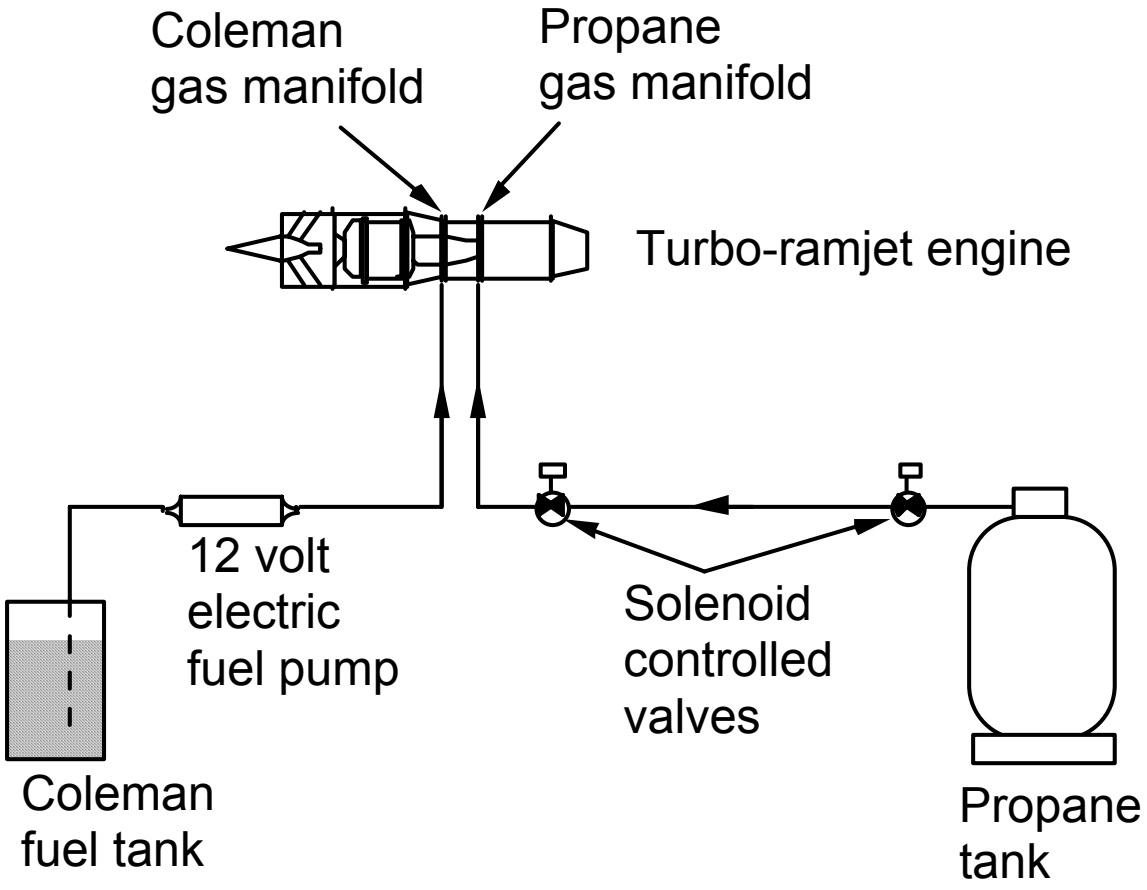

Figure 4. Afterburner Fuel System Schematic

3. Propane Pilot Burner Test Setup

The aft portion of the turbo-ramjet was removed and placed in a freestanding fashion in order to investigate propane combustion. The purpose of this test was to determine the feasibility of designing and implementing a propane pilot flame to facilitate afterburner/ramjet combustion. Propane was stored in a standard low pressure tank and a standard regulator attachment hose was used and routed from outside the laboratory inside through two fail-safe, electrically operated, solenoid valves. The propane gas was routed through the gas line to the manifold shown previously in Figure 4.

The aft duct was secured horizontally within the freejet test rig. This allowed for quick reassembly and modification if necessary. A large blower was placed upstream to simulate slow velocity flight conditions, and as a safety precaution to blow flames and unburned propane out of the laboratory through the exhaust duct.

B. DATA ACQUISITION AND REDUCTION

1. Overview

The HP9000 Series 300 workstation was used to control the data acquisition system and store the measured data. The system was well documented by al-Namani (Ref 6) and Garcia (Ref 7). Measurements were taken of net engine thrust, engine fuel flow rate, freejet plenum pressure, and static pressures at two ports in the shroud assembly. Voltages from the various sensors were acquired using a [HP6944A] DACU in conjunction with a HP digital voltmeter [DVM], which received signals through a signal conditioner. The DACU, DVM, and multi-programmer were connected to the workstation via a general purpose [IEEE-448] interface bus.

2. Instrumentation and Control

a. Thrust Measurements

The engine thrust was determined using the two beams from which the engine was suspended. Each beam contained four strain-gages [two on each side] that were configured in a full Wheatstone bridge, which were connected in parallel. The thrust signal was read through channel six on the signal conditioner panel. Prior to engine testing, the thrust beams were calibrated using the device shown by Garcia in Ref 7 in both the negative and positive directions, so as to measure both thrust and drag. Typical calibration results are provided in Appendix B as Table B1.

b. Fuel Flow Rate Measurements

The fuel flow was determined by using the existing apparatus as shown by Garcia in Ref 7. Two strain gages configured in a half Wheatstone bridge were used on the cantilevered beam to measure the fuel tank weight. The signal from the bridge was provided to the data acquisition system through Channel 0 at the signal conditioner panel. The data acquisition system took measurements of the current fuel tank weight over a constant time interval. The change in fuel weight was calculated which gave the fuel flow rate. Prior to engine testing, the beam was calibrated using known weights, the results of which are provided in Appendix B as Table B1.

c. Freejet Measurements

The engine inlet Mach number was determined by measuring the total pressure in the duct upstream of the freejet nozzle. The pressure was measured using a calibrated pressure transducer which measured the total pressure in the duct. The ambient pressure was measured in the room using a standard wall-mounted barometer. The total pressure was the sum of ambient pressure and the pressure measured by the transducer. Rearranging the expression below

$$\frac{P_t}{P_{amb}} = (1 + \left(\frac{\gamma - 1}{2}\right) M^2)^{\frac{\gamma - 1}{\gamma}} \tag{1}$$

to get Mach number gave

$$M = \sqrt{\frac{2}{\gamma - 1}\left[\left(\frac{P_t}{P_{amb}}\right)^{\frac{\gamma}{\gamma - 1}} - 1\right]} \tag{2}$$

This allowed for the Mach number of the freejet flow to be calculated. Calibration of the pressure transducer used established a linear output of 1000 mV to 1 psid, differential pressure.

d. Pressure Measurements

Two pressure transducers were installed on the top of the support I-beam to be connected to the shroud at various locations. The transducers measured static pressure throughout the ramjet duct. These measurements were used to estimate mass flow rates throughout the ramjet. Typical calibration results are located in Appendix B as Figures 32 and 33 and tables B2 and B3.

e. Flow Visualization

Flow visualization was achieved using a video camera with zoom lens directed up the exhaust of the freejet facility at the exhaust of the turbo-ramjet. This

allowed for instant feedback of the results of any changes made to the flame holder or fuel injection assemblies, after a test run, and to document the run itself.

A video feed was provided in the lab during the last test run in order for the test conductors to see flame position and quality behind the flame holder. This allowed for adjustments to be made to the fuel/air mixture in real time.

C. FREEJET RESULTS ON SHROUDED ENGINE

1. Single Beam Thrust Measurements at 100% Spool Speed

In order to repeat the thrust measurements by Garcia (Ref 7), a freejet test on the shrouded engine was conducted. The air supply tanks were pressurized to 50 psi. The engine was started and stabilized at 100% spool speed. The air supply system valve was opened to achieve a Mach number of approximately $M = 0.5$. The Mach number of the freejet was allowed to decrease to $M < 0.2$. The duration of the test run was approximately 6 minutes. Results from this test are shown graphically below. A table of numerical values is given in Appendix C as table C1.

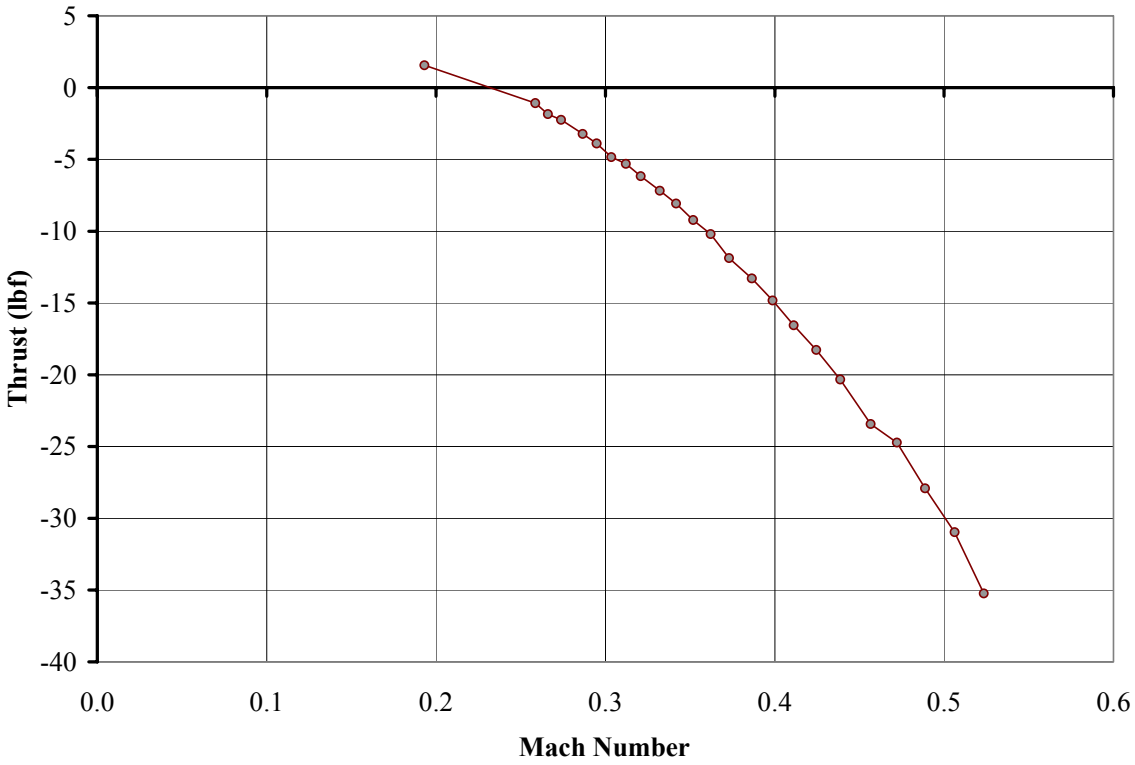

Figure 5. Single Beam Thrust Measurements at 100% Spool Speed

2. Dual Beam Thrust Measurements at 100% Spool Speed

After the addition of the second thrust beam and the two variable location static pressure transducers, a freejet test of the dual beam thrust stand was conducted. The air supply tanks were charged to 125 psi for the first run. Thrust, fuel flow, total pressure, and static pressure measurements were taken. The run lasted approximately 5 minutes after which, the tank pressure had decreased to 105 psi.

A second run was conducted to obtain measurements of thrust, fuel flow, total pressure, and static pressure at higher Mach numbers than obtained in the first run. With the lower pressure in the tanks, the valve was opened more to obtain a larger flow rate and corresponding Mach number. This run lasted approximately 5 minutes. Graphical depiction of the results is shown below. A full table of numerical measurements is located in Appendix C as tables C2 and C3.

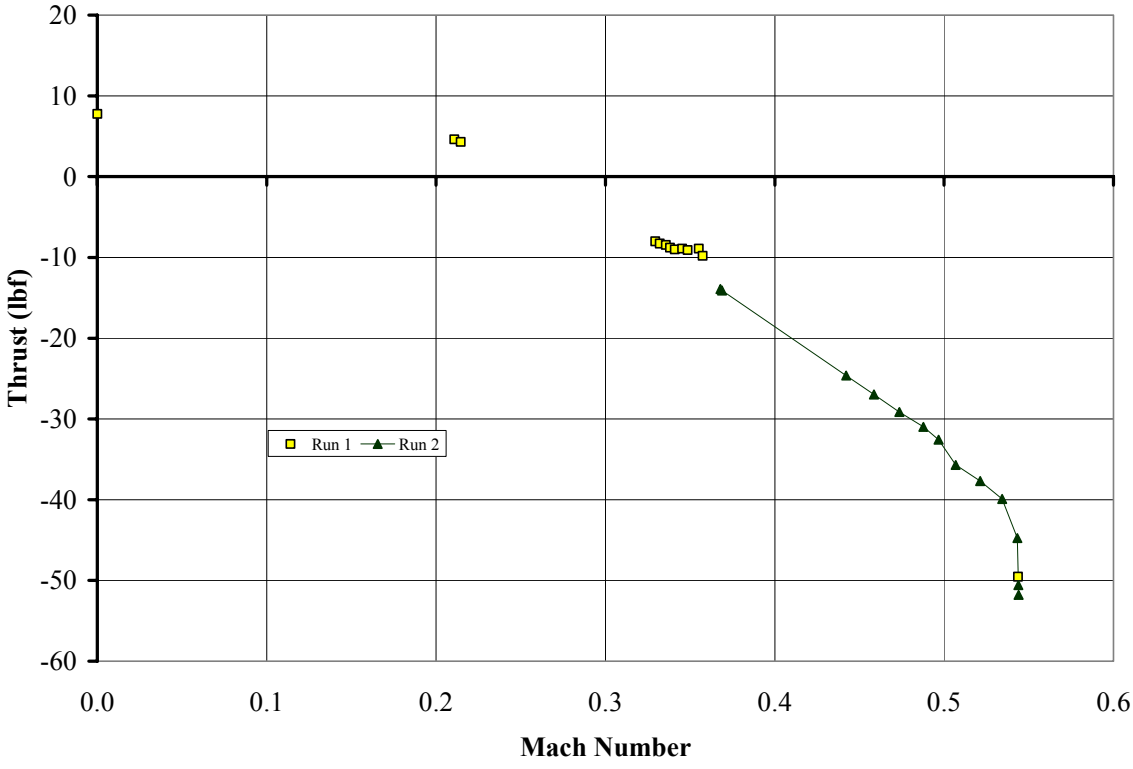

Figure 6. Dual Beam Thrust Measurements at 100% Spool Speed

3. Summary of Shrouded Engine Thrust Measurements at 100% Spool Speed

Shown below is a plot of net thrust vs. Mach number for both the single beam and dual beam runs. Also included are the results by Garcia in Ref 7 for his run on 19 August 2000.

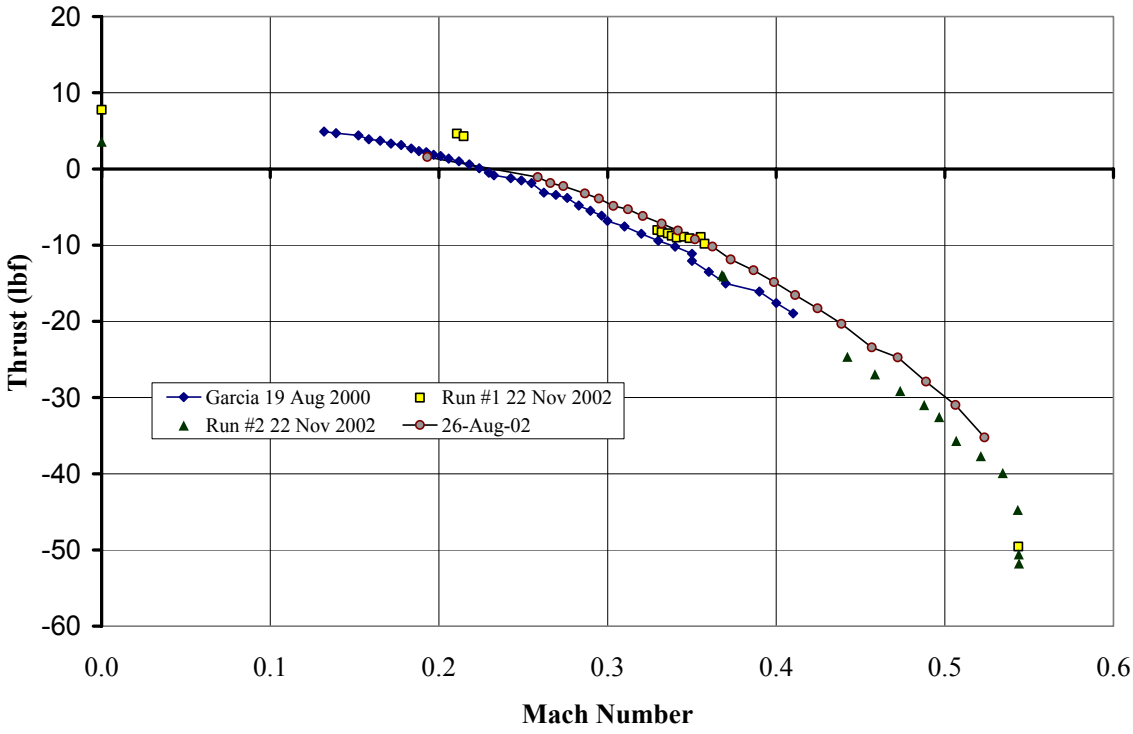

Figure 7. Shrouded Engine Thrust Measurements at 100% Spool Speed

The results from all four runs were very similar. The addition of the second thrust beam did not significantly change the thrust measurements. The trend in the measurement was as a result of the difference between the positive thrust vs. Mach number of the J450 engine and the negative drag vs. Mach number of the intake spike as calculated by Garcia in Ref 7 as Figure 19.

4. Mass Flow Rate and Velocity Calculations

The test run on 22 November had the primary purpose of verifying the changes to the thrust measuring system. The secondary purpose was to measure pressure at two locations on the shroud to calculate total mass flow rate through the shrouded engine as shown in Figure 8.

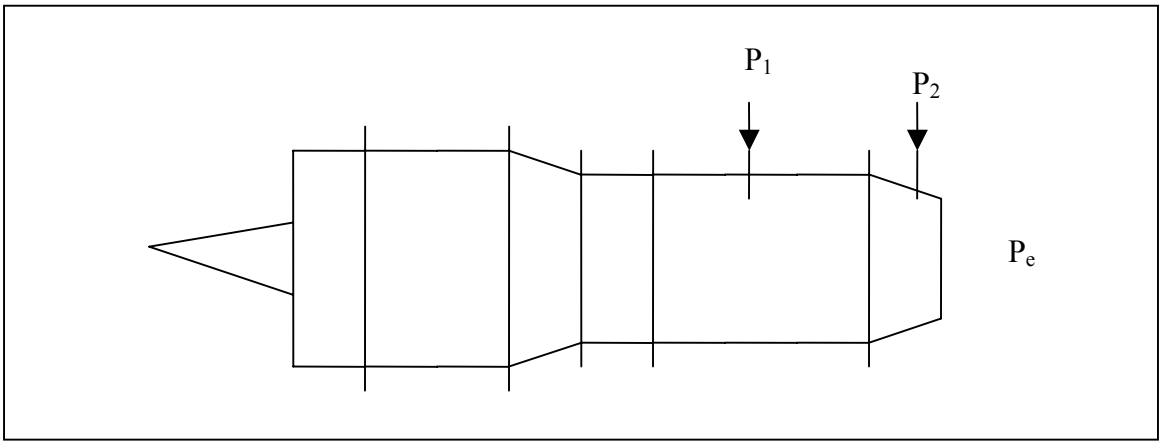

Figure 8. Schematic of Pressure Measurement Locations

The Bernoulli equation

$$P_m + \frac{1}{2g_c}\rho V_m^2 = \text{constant} \tag{3}$$

can be applied to describe the flow through a convergent nozzle as shown in Figure 9.

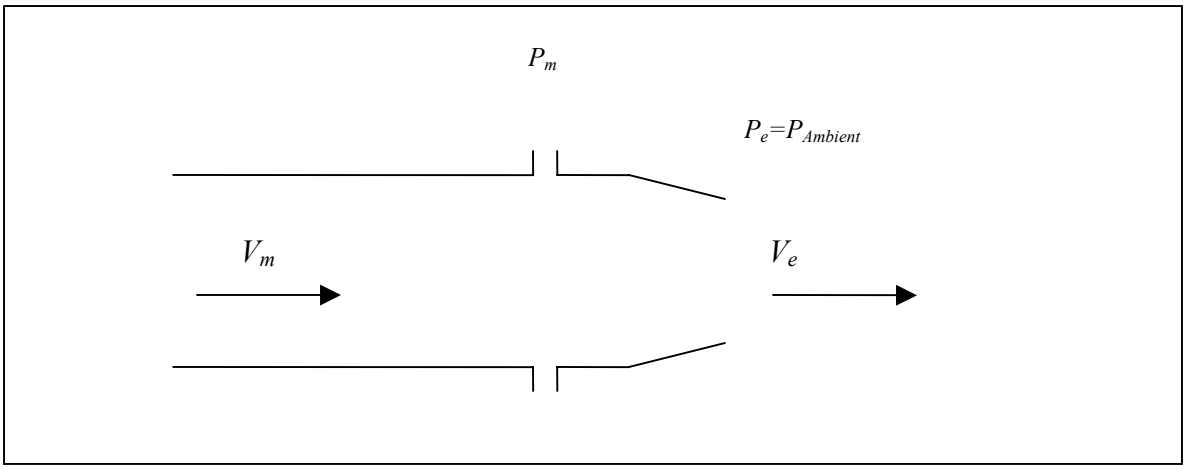

Figure 9. Pressure Measurement Diagram

Applying equation (3) to the flow between the duct and exit planes, the equation becomes

$$P_m + \frac{1}{2g_c}\rho V_m^2 = P_e + \frac{1}{2g_c}\rho V_e^2 \tag{4}$$

The m subscript denotes the location where pressure was measured either at location P_1 or P_2. Rearranging and defining ΔP_m as the pressure measured by the transducers the equation becomes

$$\Delta P = P_m - P_e = \frac{1}{2g_c}\rho\left(V_e^2 - V_m^2\right) \tag{5}$$

Density ρ was assumed to be constant, $\rho_1 = \rho_e$ so the continuity equation $\dot{m} = \rho A V = \text{constant}$ becomes

$$A_m V_m = A_e V_e \tag{6}$$

or

$$V_m = \left(\frac{A_e}{A_m}\right) V_e \tag{7}$$

Substituting for V_m,

$$\Delta P = \frac{1}{2g_c}\rho V_e^2\left[1-\left(\frac{A_e}{A_m}\right)\right] \tag{8}$$

and therefore

$$V_e = \sqrt{\frac{\frac{2}{\rho}\Delta P g_c}{\left[1-\left(\frac{A_e}{A_m}\right)^2\right]}} \tag{9}$$

For one-dimensional isentropic flow, the nozzle has a discharge coefficient, C_d of 1. Nozzles typically have a discharge coefficient between 0.9 and 1 where the steady flow continuity equation becomes

$$\dot{m} = C_d \rho A V \tag{10}$$

with C_d assumed to be .95 for the shrouded turbojet nozzle.

Equation (9) was used to calculate the exit velocity V_e and the total exit mass flow rate was calculated using equation (10). The mass flow of the engine core was approximated by using calculated off-design values from GASTURB (Ref 8). The mass flow of the bypass flow was determined by subtracting the core flow from the total flow. Total temperature of the flow in the duct was calculated iteratively using

$$T_{t7} = \frac{\dot{m}_6 C_{p6} T_{t6} + \dot{m}_{6'} C_{p6'} T_{t6'}}{\dot{m}_7 C_{p7}} \tag{11}$$

where stations 6 and 7 are depicted in Figure 10.

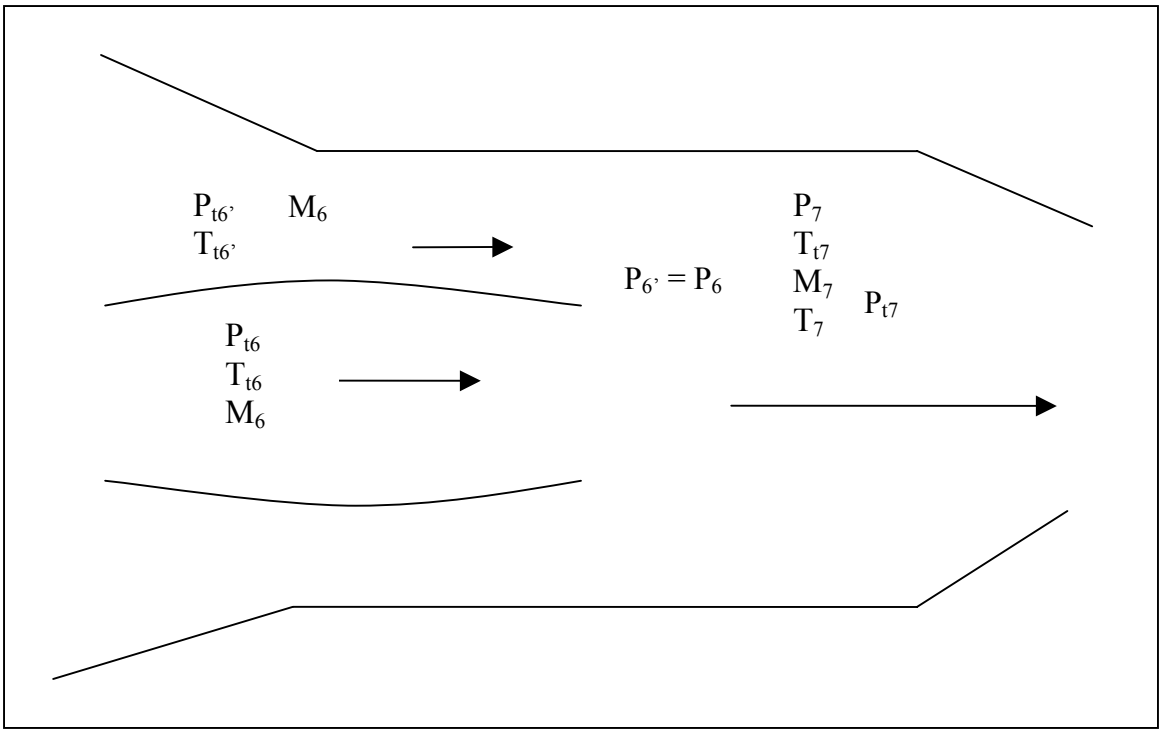

Figure 10. Mixing Model Diagram

The total temperature in the bypass duct, $T_{t6'}$ was assumed, as was an initial value for specific heat at station 7. V_7 was calculated using equation (7) and static temperature in the duct was then determined using

$$T_7 = T_{t7} - \frac{\gamma - 1}{2} \frac{V_7^{\,2}}{\gamma R} \tag{12}$$

Exit plane density, ρ_7 was then calculated using

$$\rho_7 = \frac{P_7}{RT_7} \tag{13}$$

with P_7 as the pressure measured at P_1 in the duct as shown in Figure 8. Specific heats were recalculated using the new value of temperature. Since a closer approximation of density was calculated, the exit velocity was recalculated. This algorithm was continued until convergence. Figure 11 depicts calculated total mass flow rate. Mdot 1 was the

calculated mass flow based on the measured pressure at port 1. Appendix D contains a sample calculation at Mach = 0.212 and a complete table of mass flow calculations as Table D1.

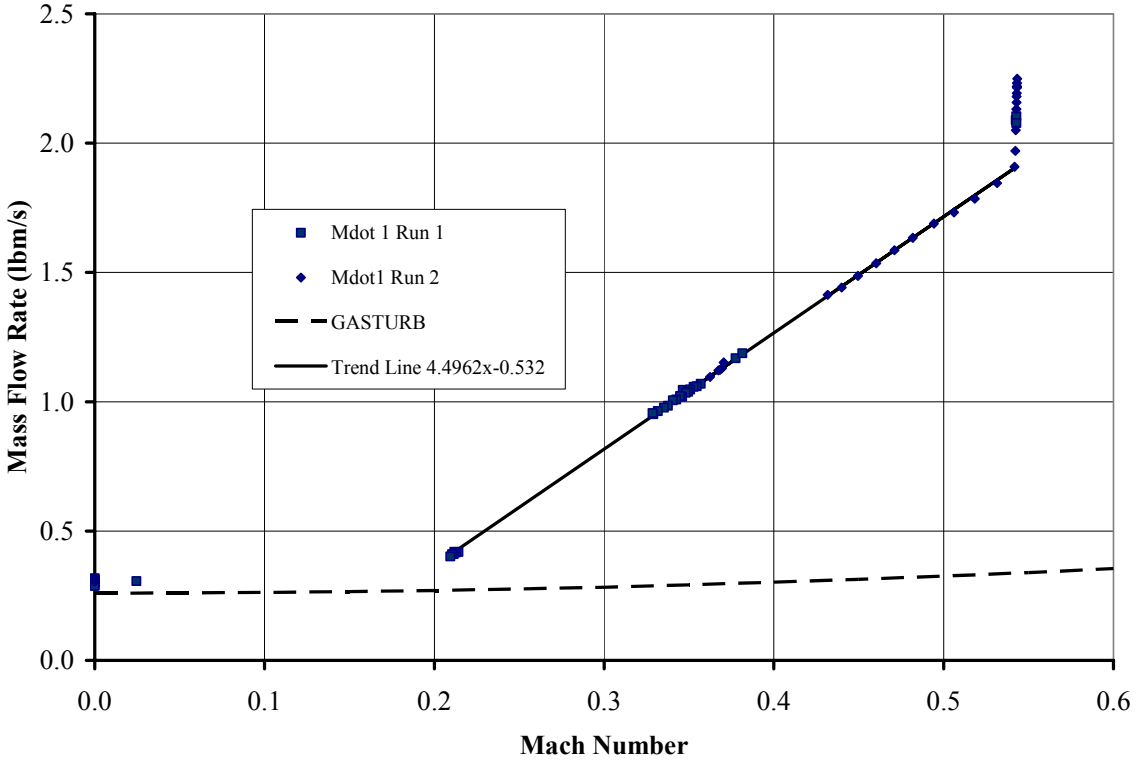

Figure 11. Calculated Mass Flow Rate Through Shrouded Engine at 100% Spool Speed

A line was fit through the data from Mach 0.2 to Mach .54. The non-linearity in mass flow rate at Mach 0.54 was due to a transient condition. During both runs the freejet control valve was opened from a lower Mach number of 0.35 or 0.2 to the larger value of Mach 0.54. The large increase in total pressure on the engine caused the momentary spike in measured pressure in the duct. After the transient condition settled, the total mass flow rate through the engine was linear below Mach 0.54. This phenomenon also occurred when opening the control valve from static conditions to Mach 0.35 but was not as pronounced. The trend line was used with the predicted values of mass flow rate of the J450 from GASTURB, and the resulting bypass ratio was calculated and shown in Figure 12. Bypass ratio was defined here as the ratio of mass flow rate through the bypass shroud duct to the engine mass flow rate.

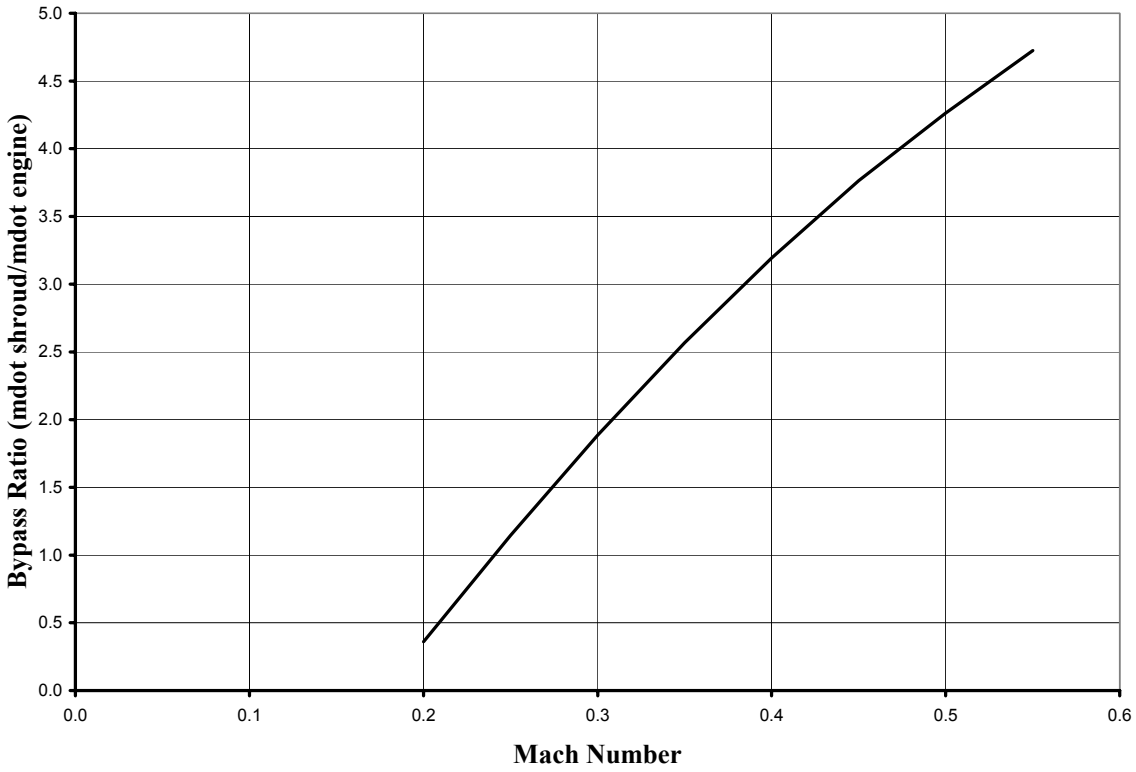

Figure 12. Predicted Bypass Ratio for Shrouded Turbojet

D. AFTERBURNER DESIGN AND DEVELOPMENT

1. Overview

The data acquired from the freejet run on the shrouded engine and resulting calculations provided the prerequisites necessary to design the afterburner/ramjet combustor. The afterburner design consisted of four separate items: afterburner duct size, flame holder size and geometry, fuel delivery method, and ignition source. An initial afterburner fuel delivery manifold or spray bars, were previously designed and tested by Garcia (Ref 7). These had to be further developed during this research and the remaining items were designed, developed, and tested.

2. Afterburner Sizing

The sizing of the afterburner was completed using the existing shroud diameter of 4.5 inches as tested by al-Namani (Ref 6) and Garcia (Ref 7). The length of the combustor duct was determined using Figure 13 taken from Mattingly (Ref 9).

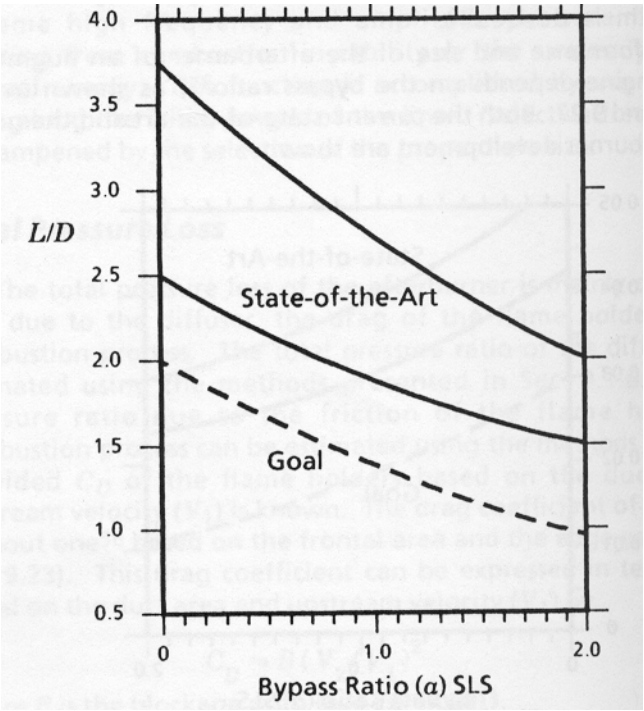

Figure 13. Afterburner Size (From Ref 9)

Figure 13 shows the ratio of the length of the combustor duct to duct diameter, $\frac{L}{D}$, as a function of mass flow bypass ratio at sea level standard conditions for a mixed flow turbofan. The assumption was made to approximate the cycle of the turbo-ramjet as a mixed flow turbofan with an outer fan pressure ratio of unity. The resulting calculations of mass flow rate in Figures 11 and 12 showed that the bypass ratio was near 0.5 at a Mach of 0.2 and increased to a value of 4.75 at a Mach of 0.54. As a result, a value of 1.5 for L/D was selected as a design starting point. This resulted in the length, L, of the afterburner to be 6.75 inches. Two shroud lengths were available for the combustor, 6 inches or 9 inches. The shorter was selected based on the premise that the nozzle section

was 3 inches in length and testing by al-Namani (Ref 6) demonstrated maximum net thrust by the J450 turbojet without afterburner.

3. Initial Flame Holder Design

The initial design of the flame holder manifold was also based on information presented in Mattingly (Ref 9). A vee gutter geometry with a half-angle of 15 degrees and an area blockage ratio, *B*, of 0.30 was selected. Much testing had been done on that configuration which gave the largest probability of flame stabilization with reasonable total pressure losses. The vee gutter design is shown in Figure 14.

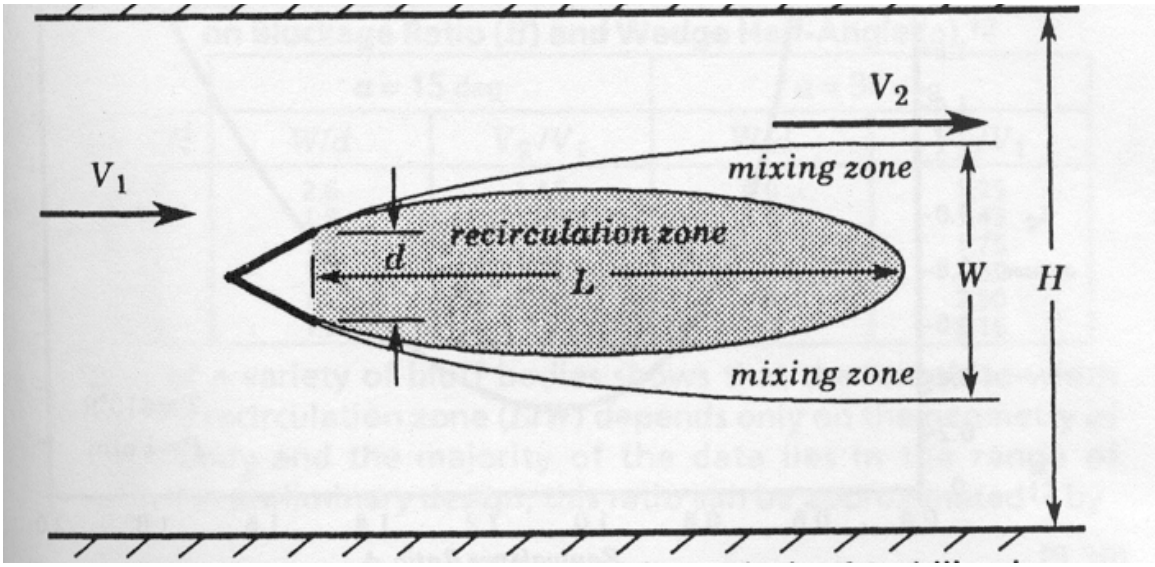

Figure 14. Flame Holder Design Diagram. [From: Mattingly (Ref 9)]

Typical flame holder used in analysis of stabilization where

V_1 = Velocity of approaching stream

V_2 = Velocity of flow at edge of mixing zone

d = Width of the flame holder

L = Length of the recirculation zone

W = Width of the wake

H = Width of duct

The analysis is typically applied to a 2-dimensional duct where the blockage ratio

$$B = \frac{d}{H}. \tag{14}$$

However since the afterburner duct was circular, the blockage ratio was taken as the area blocked by the flame holders. This analysis was valid as Mattingly stated that the same analysis used for 2-D ducts can be applied to axi-symmetric ducts. The width of the flame holder, *d*, needed to be calculated first. The cross-sectional area of the duct was

$$A = \pi r^2 = \pi\left(2.25\right)^2 = 15.904\ \text{in}^2$$

(15)

The resulting cross sectional area of the flame holder (30% of total area) was calculated to be 4.77 in^2. The center of the flame holder in the circular duct was desired be at a radius of 1 inch from the center of the duct. The inner and outer diameters of the flame holder were calculated using equation 16.

$$A_{flameholder} = \pi\left(r_{outer}^2 - r_{inner}^2\right) = \pi\left[(1+x)^2 - (1-x)^2\right] = 4.77in^2$$

(16)

The value of x was determined to be 0.38 inches. The width of the flame holder, d became

$$d = 2x$$

(17)

$$d = 0.76\ \text{inches}$$

This led to the flame holder outer diameter of 1.38 inches and an inner diameter of .62 inches. Table 9.4 from Ref 7 gave the ratio of wake width with respect to flame holder width for a wedge half-angle of 15 degrees and blockage ratio, B of 0.3 to be

$$\frac{W}{d} = 1.3$$

$$W = 0.988\ \text{inches}$$

Ref 7 further states that the recirculation zone L can be approximated as

$$\frac{L}{W} = 4$$

or

$$L = 3.952\ \text{inches.}$$

The initial flame holder assembly is shown in Figure 15.

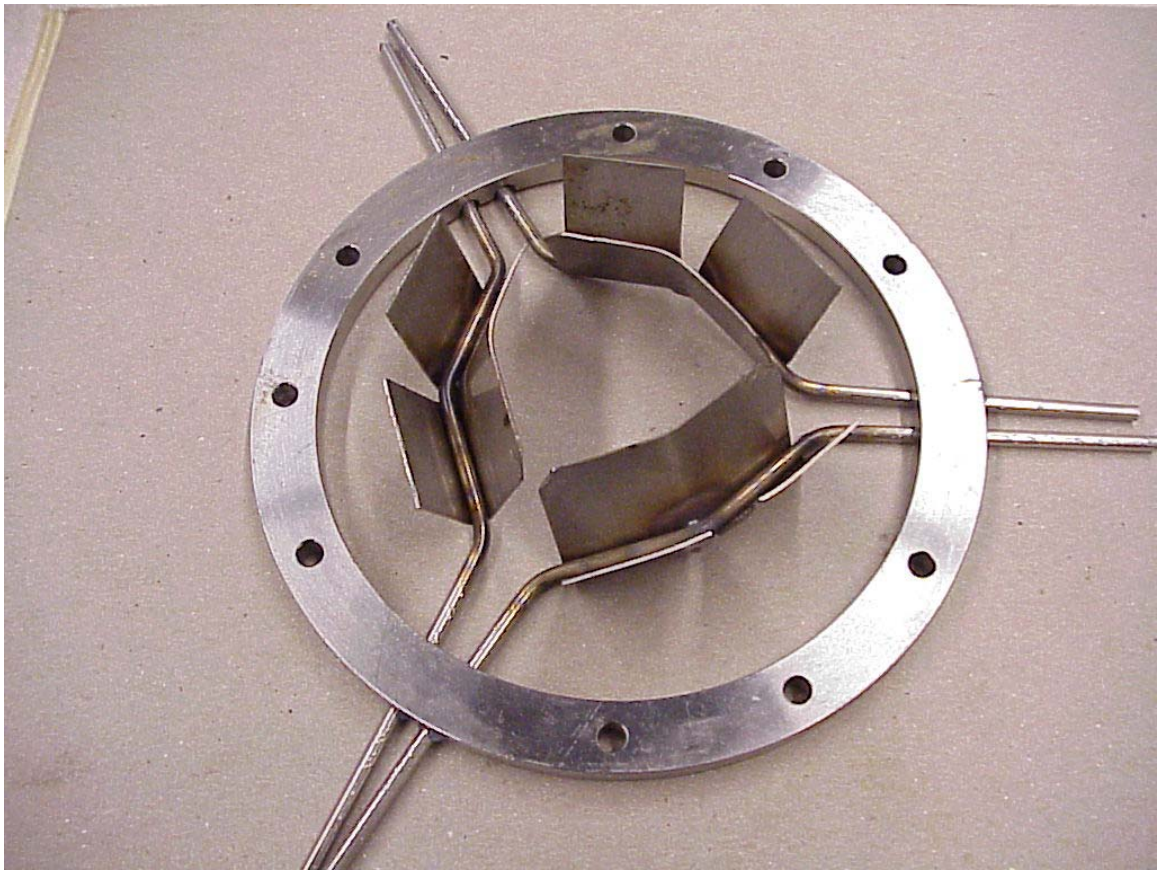

Figure 15. Initial Flame Holder.

The flame holder was initially placed 3 inches downstream of the fuel injection system. A J450 turbojet spark plug was placed approximately one half inch downstream of the flame holder.

The initial configuration was unsuccessful. It was determined that either the fuel had not atomized and/or vaporized enough for ignition, the spark plug did not create a large enough ignition source, or the fuel air mixture was not close enough to stoichiometric behind the flame holder in the recirculation regions. Further research revealed that numerous military aircraft afterburning engines use a pilot flame, or torch igniter, to ensure afterburner light off.

4. Propane Pilot Flame Design

To create a pilot flame behind the flame holder manifold, a fuel injection manifold was placed within the flame holder. This would ensure that there was a proper

fuel/air mixture behind a localized area of recirculation and low Mach number. The Coleman Fuel/Kerosene mixture used previously was replaced with propane gas to ensure combustion at standard pressure and temperature. The aft portion of the turbojet was removed from the engine test rig and placed horizontally on a bench. The flame could be observed through the nozzle upstream and downstream to the back of the flame holders to obtain qualitative information for further development.

Initial testing consisted of a manual valve opened up slowly until ignition was achieved using a spark igniter. Once ignition was successful, an external blower was added upstream to simulate low mass flow, low Mach number conditions. Once a stable flame in the duct was accomplished using the external blower, the duct was replaced on the engine.

The pilot flame was lit initially using the external fan and the manual propane control valve without the engine running. The external fan created a large enough flow through the engine to maintain the flame downstream of the turbojet engine. Engine starting air was then used to spin the turbojet to observe the effects of engine exhaust on the pilot flame. With the maximum amount of starting air placed on the compressor, the pilot flame remained stabilized in position. The engine was then started. As the engine spooled up, the flame blew out. It was determined that a larger fuel flow would be required. After the test, the videotape from the downstream camera revealed a large amount of swirl exiting from the turbojet. This created a very large shearing effect and compounded the difficulty of flame stabilization.

The initial propane manifold had 9 holes at 0.013 of an inch. Since the extinguished flame was blue in color the indication was that the flame was lean, hence more fuel was needed to keep the pilot flame lit during engine start up.

New spray bars were developed with 24 larger holes at .050 of an inch spraying propane radially inward and outward within the final flame holder. This configuration worked well, but a larger mass flow rate was still needed. Two constriction points in the supply line were removed to give the current configuration (Figure 4).

5. Final Flame Holder Configuration

The large swirl caused by the turbojet exhaust made flame stabilization difficult. In order to minimize the effect, a new flame holder was designed and implemented. The final flame holder inner radius was circumferentially continuous. This eliminated the effect of the large swirl from the turbojet entering the recirculation zone as previously occurred on the initial flame holder. The final flame holder was also more uniform in appearance and eliminated asymmetries in the afterburner duct. The final flame holder configuration is shown in Figure 16.

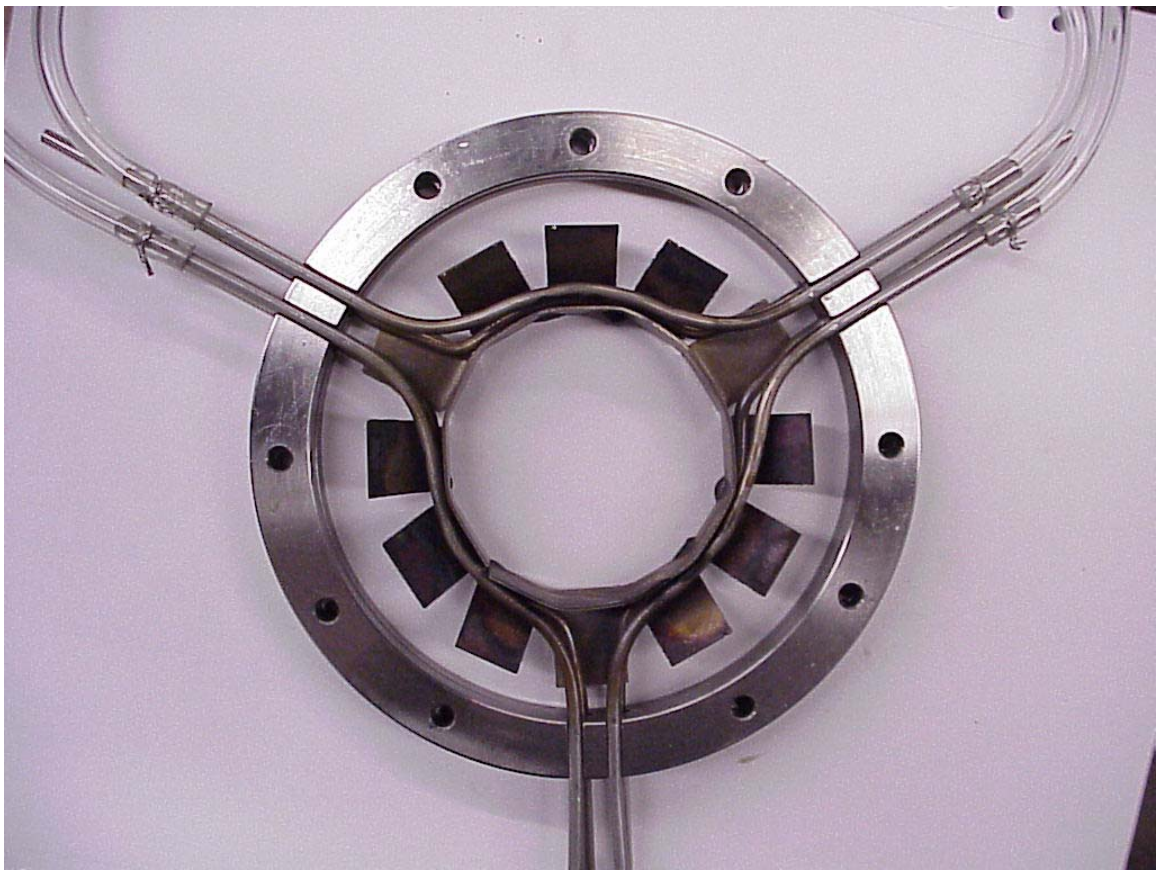

Figure 16. Final Flame Holder Configuration with Pilot Flame

The J450 spark plug was not long enough to be positioned directly within the recirculation zone of the flame holder. This made pilot ignition difficult. A final modification to the flame holder assembly was the addition of a longer spark plug. The longer spark plug was also shielded from direct exposure to the flow and the spark was

placed directly behind the flame holder. The spark plug was within close proximity of the propane pilot manifold, which facilitated ignition.

6. Coleman Fuel Manifold

Once the pilot flame and flame holder were successfully tested, a Coleman fuel manifold was added 3 inches upstream of the vee gutters. This fuel system was driven by an additional 12V fuel pump. This fuel manifold had 12 injection ports spraying radially inward onto the hot turbojet exhaust, which vaporized the Coleman fuel. Figure 17 shows the manifold installed over the engine exhaust. The final turbo-ramjet configuration is shown in Figure 18.

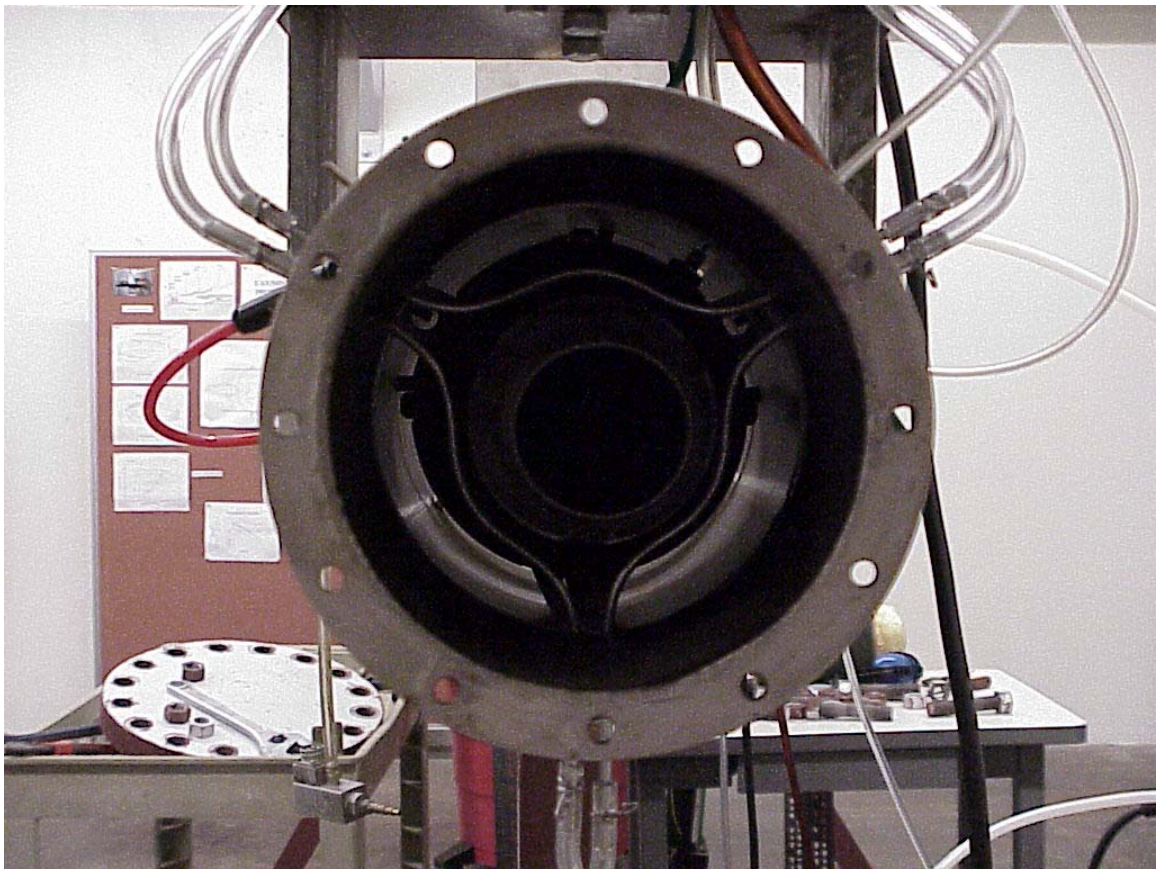

Figure 17. Coleman Fuel Manifold Installed on Turbo-Ramjet

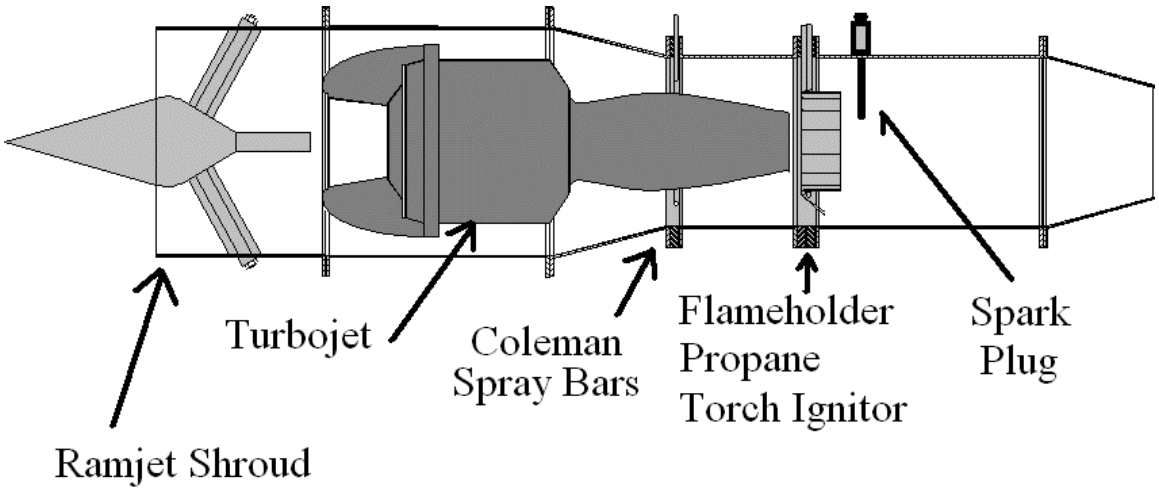

Figure 18. Schematic of the Final Turbo-Ramjet Engine Configuration

E. FREEJET RESULTS ON TURBO-RAMJET

1. Afterburner Results

The turbo-ramjet was tested three times in the final configuration. The initial test run was conducted to test the engine with the afterburner running, however, little control of the freejet flow rate was possible. The control of the freejet flow rate was improved by including a digital readout of the plenum pressure to the operator of the air supply system control valve. Once the turbojet was running at 80% spool speed with sustained afterburner, the freejet was started and the Mach number gradually increased. Fuel was added to maintain stable combustion in the burner. The turbojet ran successfully at static conditions with the afterburner running, however with a decrease in net thrust. This was most likely due to the large back pressure placed on the turbojet by the afterburner. With the freejet running, the turbo-ramjet maintained positive net thrust from static conditions to Mach 0.2 as shown in Figure 19.

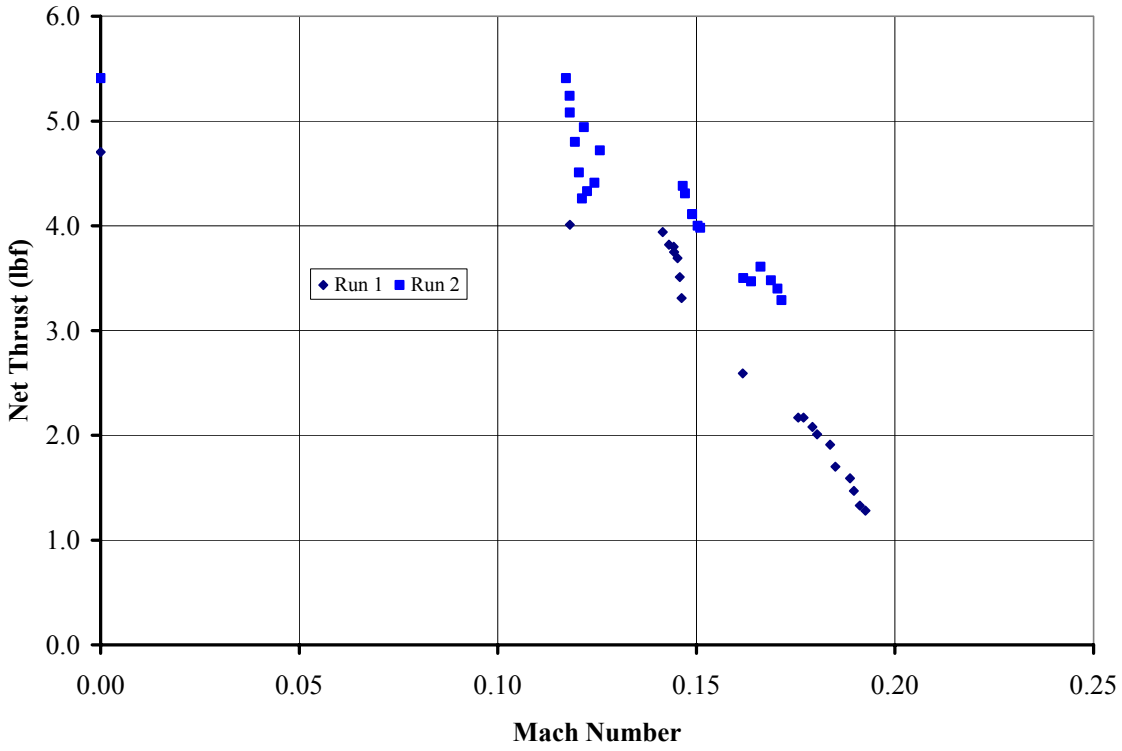

Figure 19. Thrust Measurements with Afterburner at 80% Spool Speed

2. Afterburner Results Comparison with Shrouded Turbojet at 80% Spool Speed

Figure 20 depicts measured net thrust vs. free stream Mach number with the turbojet running at 80% spool speed. Tests were also conducted by Garcia (Ref 7) of the shrouded engine at varying engine spool speeds. These values are tabulated in Appendix E as Table E3. Garcia's results at 80% spool speed are compared to the net thrust results of the turbo-ramjet running with afterburner. It can be seen that on average there was a net increase of three pounds thrust up to Mach 0.2. This equated to a 40% increase in thrust over the baseline J450 at 80% spool speed. This was equal to the typical increase in thrust experienced by conventional afterburning turbofan and turbojet engines.

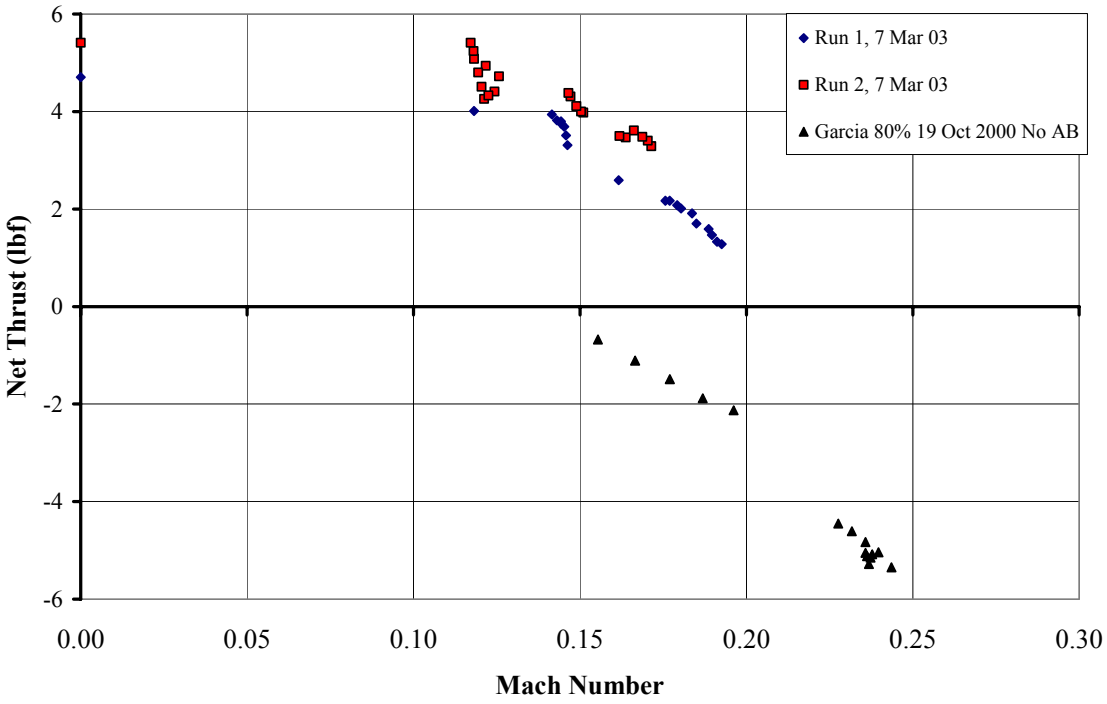

Figure 20. Comparison of Afterburner vs. Non-Afterburner at 80% Spool Speed

The values of thrust approaching a Mach number of 0.2 are misleading. At this Mach number, the fuel pump did not supply adequate fuel to maintain a proper fuel air ratio in the afterburner. During this time it was noted that the flame was only on one section of the flame holder. Beyond Mach 0.2 the flame in the afterburner was extinguished thus a larger fuel pump is needed to extend the range of the turbo-ramjet. The calculated mass flow rate through the shrouded engine depicted on Figure 11 shows a small increase in total mass flow rate through the turbo-ramjet up to a Mach number of 0.2. The amount of bypass flow that was combusted at these speeds was relatively small (0.5 bypass ratio) compared with the J450 mass flow rate. Shown in Figure 21 is the turbo-ramjet engine running at 80% spool speed with full afterburner at $M_\infty = 0.15$.

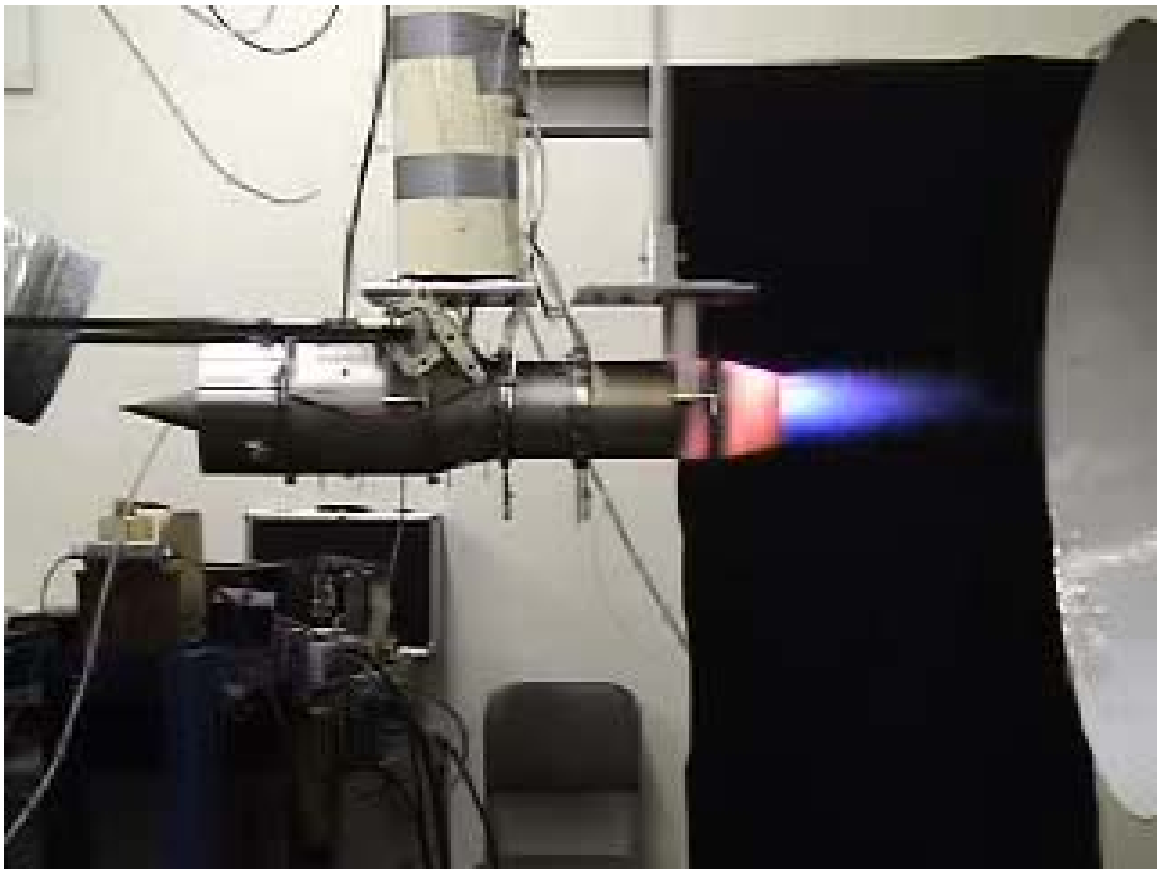

Figure 21. Turbo-Ramjet at Maximum Afterburner at $M_\infty = 0.15$

III. COMPUTATIONAL FLUID DYNAMICS ANALYSIS

A. BACKGROUND

Computational Fluid Dynamics (CFD) is widely used in aeronautics as a modern engineering design tool. The Naval Postgraduate School (NPS) currently supports numerous software applications for applied engineering science using Silicon Graphics Workstations. The purpose of using CFD was to obtain solutions to the internal flow field of the turbo-ramjet and to compare these results to experimental and analytical results. One of these software codes is the NASA supported CFD code OVERFLOW (Ref 10) that NASA uses extensively for modeling Space Shuttle vehicle aerodynamics. OVERFLOW has been applied to numerous single- and multi-block grid geometries at various flight conditions at NPS.

Modeling of the internal flow of the turbo-ramjet engine was accomplished using OVERFLOW. A two-dimensional planar grid was generated using the grid generation software GRIDGEN. The points were exported from GRIDGEN to be manipulated upon by the code GRIDED.

Four computational grids were created for use in OVERFLOW. All grids were C-type axi-symmetric grids. Part of the outer boundary of the grid was set as the ramjet shroud, which allowed for the simulation of the internal flow field. From prior analysis, the results from an internal/external flow solution and an internal only solution did not differ. Solving for the internal flow allowed for less required computational time and required fewer boundary conditions to be specified.

Simple test cases of a ramjet with nose-cone shroud and a cylindrical pipe were run to ensure no difference in the solutions between internal only and internal/external solutions.

Even with the change of an internal only flow solution, convergence of solutions for a free stream Mach number below 0.6 were unattainable.

B. SOFTWARE

1. GRIDGEN

GRIDGEN is software for the generation of 3D, multiple block, and structured grids. The code may also be used to generate single block structured grids, single surface structured grids, and overset structured grids. The Version 9 of the software system was used during the current research. The code can be used to convert a 3D domain into blocks, distribute grid points on curves, initialize and refine grid points on surfaces, and initialize volume grid points. The code was written using the Silicon Graphics Iris GL graphics library and hence may only be run on Silicon Graphics 4D Series and IBM RS/6000 Series workstations.

2. GRIDED

GRIDED is a grid editing software package. This powerful code can do many manipulations to existing 2D and 3D grids. For the purpose of this thesis, this tool was used to interchange the J and K grid families of the single input grid generated from GRIDGEN and to generate two additional planes that were supplied to OVERFLOW to solve the axi-symmetric flow field.

3. OVERFLOW

OVERFLOW is a Navier-Stokes flow solver for structured grids. First-order implicit time stepping was used. A time-accurate mode is available, or local time step scaling can be selected for acceleration to steady state. A more complete description of the flow solver and implementation examples were documented by Coyne in Ref 11, Garcia in Ref 7, and Williams in Ref 12.

4. FAST

FAST is a software environment for analyzing Computational Fluid Dynamics data. FAST consists of a collection of separate programs (modules) that run simultaneously and allowed the user to examine the results of numerical simulations by loading grid and solution data files. Calculations could be performed on the solution for flow visualization which may be animated and recorded.

C. RESULTS

1. Ramjet Shroud with Nose Cone

The first configuration modeled was a pure ramjet. The solution to this configuration provided information on the flow at the inlet area of the ramjet. A test case was run with free stream Mach = 0.6. The grid size was a 411x51x3 grid and the extent of the shroud and inlet nose cone are shown in Figure 22. The OVERFLOW input file is listed in Appendix F.

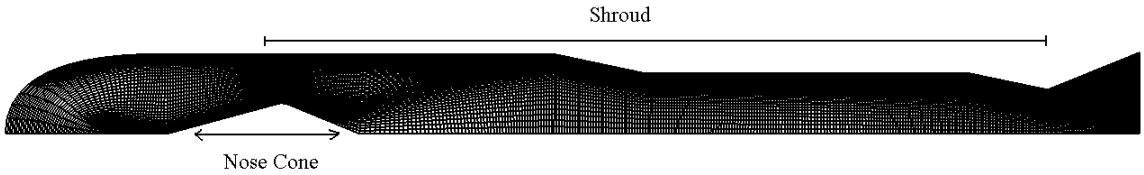

Figure 22. Ramjet Grid (411x51x3)

Garcia obtained a supersonic solution at Mach 2 for the inlet only. He had to guess the amount of back pressure within the shroud, hence making his calculations suspect. The present full shroud simulation allowed for the opportunity to analyze the flow through the duct and determine the amount of spillage caused by the nosecone and shroud back pressure at subsonic speeds. A solution was obtained at a free stream Mach number of 0.6. The solution was obtained after 10,000 iterations and reached 3 orders of magnitude convergence as documented by the L2 norm residuals plot in Appendix F.

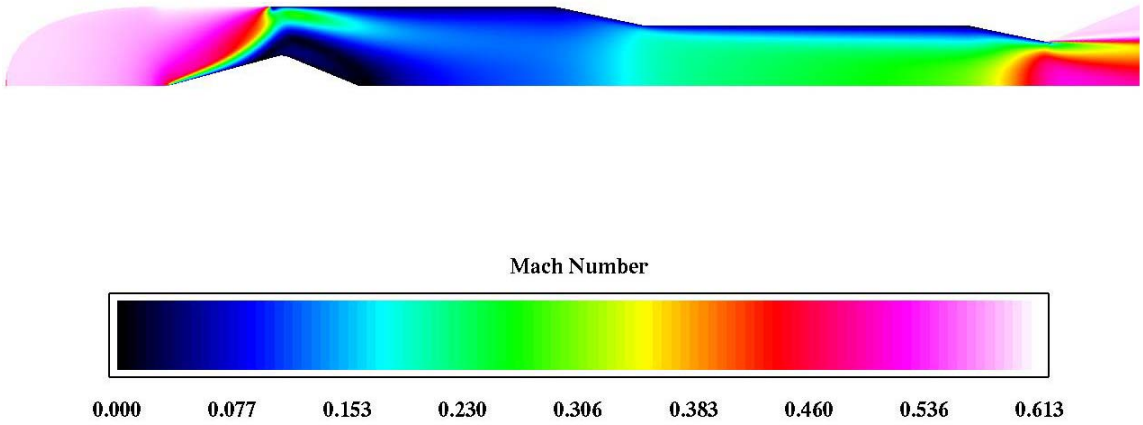

Figure 23. Mach Number Distribution through the Ramjet at $M_\infty = 0.6$

As can be seen in Figure 23, the majority of inlet flow bypassed around the ramjet. The remaining flow accelerated through the duct and exhausted at slightly less than free stream Mach number. The conical engine inlet was designed by al-Namani (Ref 4) and was optimized at Mach 2. The Mach 0.6 results from OVERFLOW showed a large amount of spillage caused by the nose cone and a large area of recirculation developed downstream of the conical inlet.

2. Turbo-Ramjet Geometry with Inflow and Outflow Through the Turbojet

The grid used was 556x51x3 in size. As shown in Figure 24, the J450 engine inlet was modeled as a constant pressure outflow with the pressure adjusted to allow for the proper mass flow rate into the turbojet. The exhaust nozzle of the J450 was modeled as a nozzle inflow at free stream conditions. The exit velocity of the turbojet was the same as the free stream Mach number as shown in Figure 25, and the exhaust gasses in the solution were cold as opposed to the hot exhaust in the experiment.

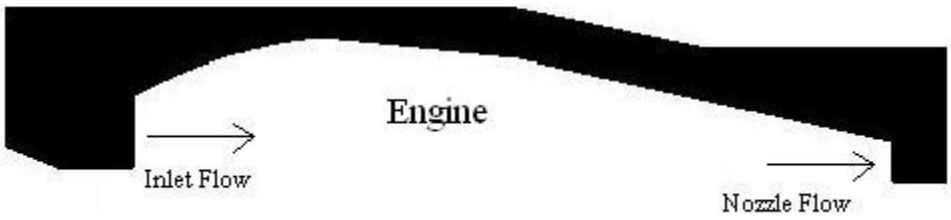

Figure 24. Turbo-Ramjet Grid with Engine Inflow/Outflow

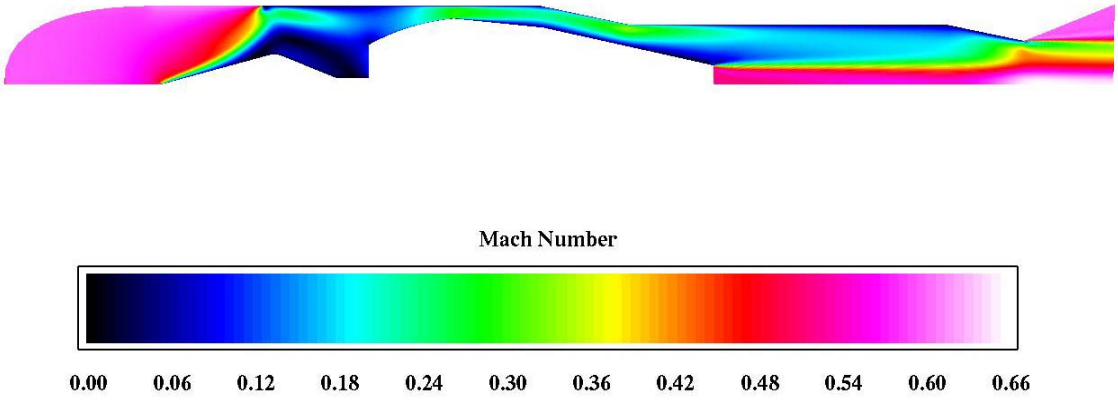

Figure 25. Mach Number Distribution for Engine Inflow/Outflow at $M_\infty = 0.6$

3. Turbo-Ramjet Geometry with Flow Through the Turbojet with an Actuator Disk and Heating

The next modeling attempt was to model the flow through the turbojet in order to produce an exit gas temperature and pressure closely resembling actual conditions. This grid was 592x109x3 in size.

The flow through the engine was modeled by using a combination of constant temperature walls internal to the engine and an actuator disk to simulate an increase in pressure through the engine as shown in Figure 26. Values from GASTURB (Table G1) were used at a free stream Mach number of 0.6 to predict exit conditions from the

turbojet to be a temperature of 1440 degrees R and a pressure of 21.5 psia. The actuator disk boundary condition in OVERFLOW required a value equal to $\frac{\Delta P}{P_\infty}$ as a specified BCPAR(1) input in the $BCINP namelist. The final value to obtain the proper exit pressure from the turbojet was 0.18. Viscous adiabatic constant temperature walls were set in the input file to produce exhaust gas temperature consistent with the predicted value of 1440 degrees. This was done through a series of iterations via trial and error. The inner boundary of the turbojet was modeled as a constant temperature adiabatic wall from just inside the engine inlet to the end of the engine exhaust at 3000 degrees R as shown in Figure 26. The outer wall of the engine casing was set as a constant temperature adiabatic wall with a temperature of 1000 deg R to model heat exchange into the bypass duct. Finally, the outer surface of the exhaust pipe of the J450 was modeled as a constant temperature adiabatic wall with a value of 1500 degrees R to simulate convective heating into the bypass flow.

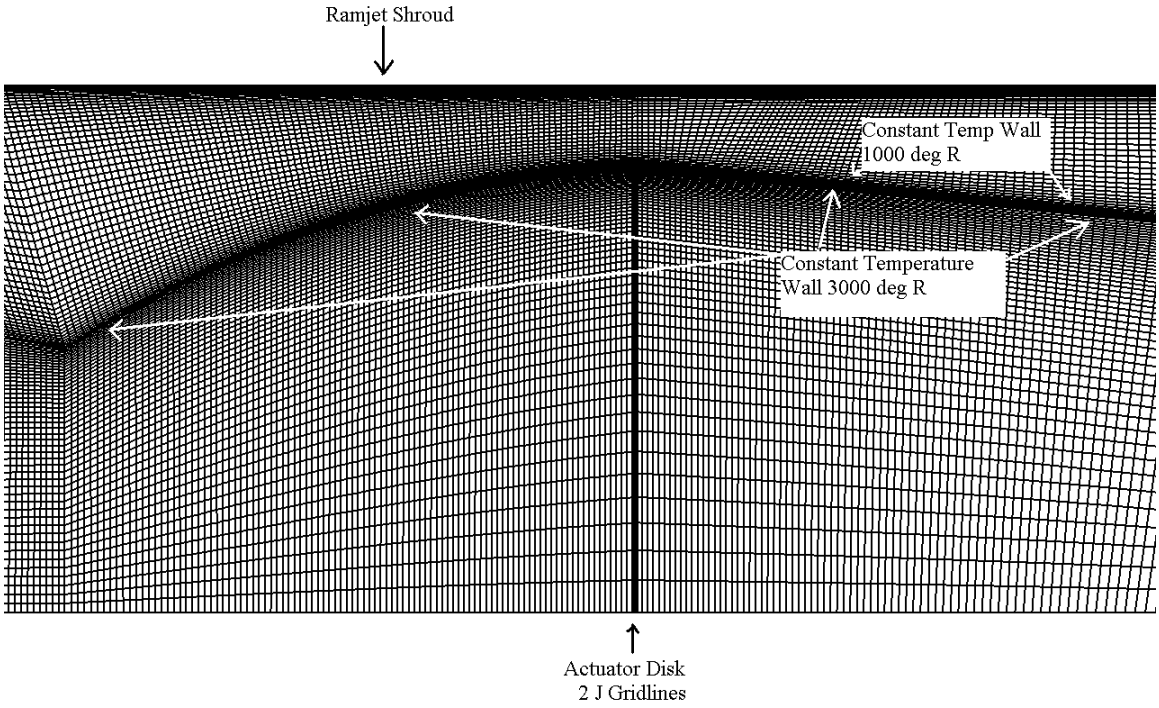

Figure 26. Close-Up of Grid with Engine Through-Flow Modeling

Figure 27 shows the Mach number distribution through the engine at M_∞= 0.6. What was of interest was the low Mach number (0.3) at the bypass duct constriction at the largest radius of the J450 engine. Also noteworthy was that the bypass flow remained at this Mach number until mixing with the J450 exhaust. At this point, the Mach number varied with respect to distance radially outward of the turbojet exhaust flow from between Mach 0.2 and 0.3. Lastly, when compared to the Mach number results of the ramjet shroud and the Engine Inflow/Outflow, the Mach number profile at the inlet was remarkably similar. In addition, the Mach profile of the Engine Inflow/Outflow and the Through Flow model from the inlet to the throat of the bypass duct were also very similar.

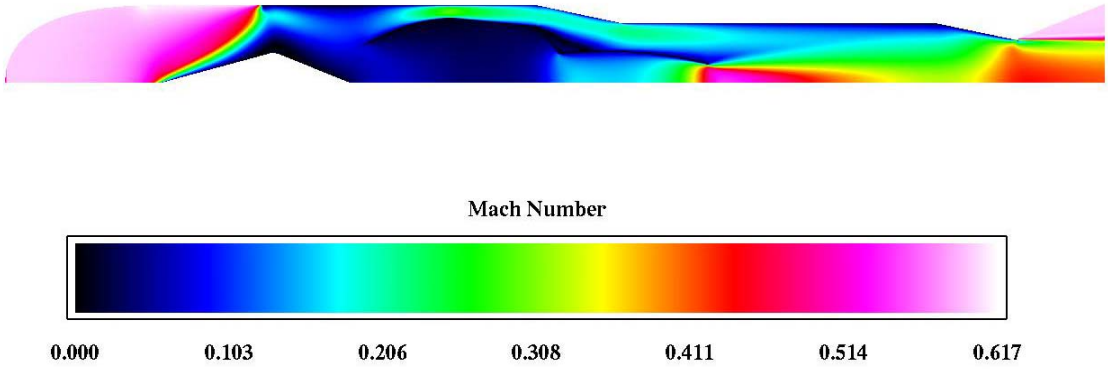

Figure 27. Mach Number Distribution for Flow Through Turbo-Ramjet at M_∞= 0.6

THIS PAGE IS INTENTIONALLY LEFT BLANK

IV. ANALYSIS OF DESIGN AND PREDICTION TOOLS

Previously discussed was the importance of flow visualization with respect to gaining a qualitative representation of the properties of the afterburner flame during operation. The CFD results of the turbo-ramjet modeling of the turbojet engine flow gave qualitative and quantitative data of the flow through the turbo-ramjet. Figure 28 shows the pressure distribution through the turbo-ramjet at $M_\infty = 0.6$.

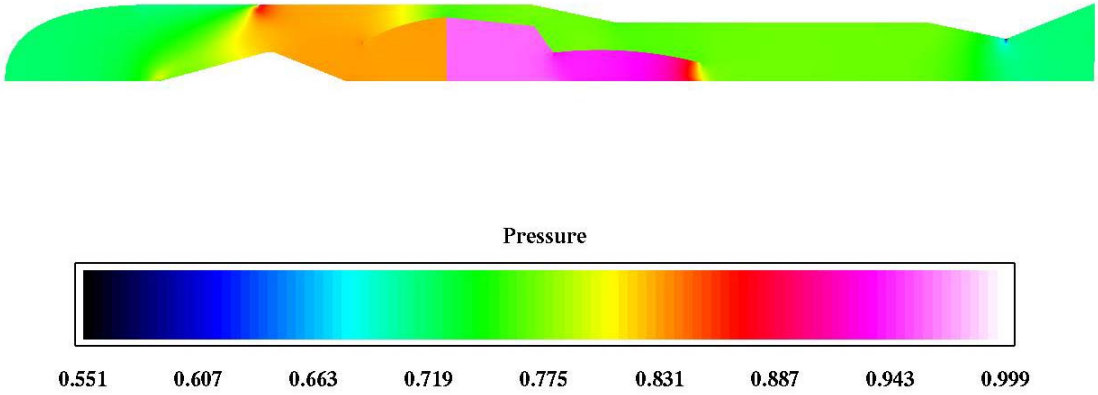

Figure 28. Pressure Distribution of Flow Through Turbo-Ramjet at M_∞=0.6

The pressure downstream of the turbojet engine exhaust was calculated to be 0.79 from Figure 28. This equated to a pressure of 16.25 psi (1.56 psig) at standard pressure in the duct at station 7 in Figure 10. The pressure measured during the shrouded engine at 100% spool speed in the freejet at $M_\infty = 0.54$ was 1.7508 psig (Table D2).

The mass flow calculations discussed in Section II.C.4 used the assumption of constant density from station 7 to exit. The density solution from OVERFLOW depicted almost constant density radially over the profile of the mixed exhaust flow. Hence, the CFD model of the shrouded engine closely simulated the actual flow through the engine with the bypass duct. The calculated bypass ratio results were then used with GASTURB to predict the performance of the turbo-ramjet as a mixed flow, afterburning turbofan engine with a fan pressure ratio of one. The GASTURB predictions are shown in

Appendix G where a thrust of 4 lbf predicted at Mach 0.2 compared favorably with the measured values of 3 lbf of increased thrust. The GASTURB output for the prediction is presented in Appendix G as Table G2.

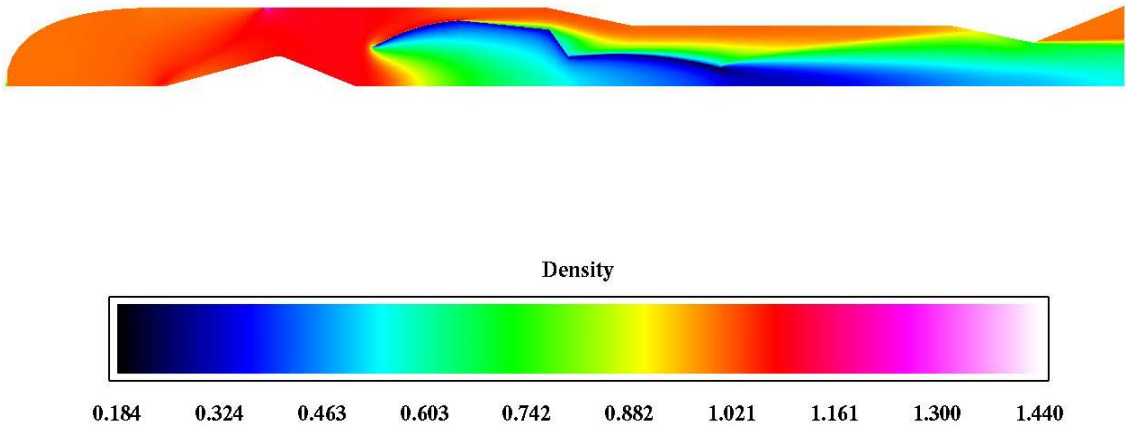

Figure 29. Density Distribution of Flow Through Turbo-Ramjet at M_∞=0.6

The pressure measurements, P_2 were taken for redundancy in measurement. The measurements cannot be applied to the constant area mixing model shown in Figure 11. The angle of the nozzle pressure port would cause a stagnation point that would cause a larger than actual measurement. At static conditions, the calculations performed with the pressure measurements from position P_1, differed as much as 20% from GASTURB predicted values. This was a result of the correct pressure not being "sensed" by the transducer as a result of the expanding exhaust from the turbojet not yet reaching the shroud wall. At static conditions calculations were performed using equation (4) and the pressure P2, as these were considered more accurate due to the expanding exhaust jet exhibiting a more uniform profile in the nozzle vice its profile upstream at position 7.

V. CONCLUSIONS AND RECOMMENDATIONS

The freejet facility was upgraded with the introduction of a second thrust beam to stabilize the engine and eliminate undesired vibration and pitching movements during high Mach number test runs. Testing of the shrouded turbojet engine was extended from Mach 0.45 to Mach 0.6, however a more capable control valve must be added to ensure subsequent successful testing at higher Mach numbers. The inability to slowly change free stream conditions during testing resulted in non-linear measurements at higher Mach numbers and afterburner flame blow out. Static pressures in the shrouded engine were measured to determine a cold-flow bypass ratio of 0.4 at Mach 0.2 and 4.75 at Mach 0.54.

A combustor was successfully designed, developed and tested for a turbo-ramjet engine. The combustor consisted of a propane pilot and vee gutter flame holder, Coleman fuel manifold, and extended spark plug. The combustor was successfully tested to a Mach number of 0.2 with stable operation during increased and decreased free stream velocities. The turbojet engine was run at 80% spool speed and with the afterburner lit an increase in thrust of three pounds was measured. The thrust increase was 40% over the baseline turbojet engine. The positioning of the video camera to view the afterburner flame during engine operation, was vital in maintaining a stable flame during changes in free stream Mach number. Although the turbo-ramjet was operating at subsonic speeds, a significant increase in thrust was measured at these low subsonic speeds. This provided optimism for future testing at higher speeds in conjunction with optimization of the flame holder. The increase in bypass flow rate from Mach 0.2 to Mach 0.54 should result in a further increase in thrust due to the combustion of the cold bypass flow. Further tests are needed with the turbojet engine running at 100% spool speed.

Further testing of the combustor cannot be completed without a higher flow rate fuel pump. The large increase in total mass flow rate calculated using the shrouded turbojet static pressure measurements demonstrate the large fuel rates needed at higher Mach numbers. One idea for future testing is to use the turbojet compressor bleed air as

the power source for the afterburner fuel pump. An improved flame holder should be manufactured more closely resembling full-scale afterburning turbojet and turbofan engines. This could result in greater combustion efficiency, and hence greater thrust at higher speeds. The ramjet shroud should be redesigned from its present convergent shape aft of the turbojet to a constant diameter duct followed by a convergent nozzle.

The gas turbine prediction program GASTURB was considered highly accurate in predicting the baseline performance characteristics of the J450 turbojet. The predicted flow parameters through the turbojet were used in conjunction with the flow solver OVERFLOW to produce a valid solution of the flow through the turbo-ramjet at M = 0.6. The computational grid should be further refined with the modeling of the flame holder. Combustion in the afterburner could then be modeled with heat addition from the flame holders. Current and future turbo-ramjet model configurations need to be computed at supersonic speeds in an attempt to assist the performance prediction of such a combined cycle engine.

APPENDIX A. SOPHIA J450 ENGINE SPECIFICATIONS

SOPHIA J450 ENGINE SPECIFICATIONS	
Length/Diameter	*13.19/4.72 [in]*
Total weight	*4 [lb]*
Fuel	*Coleman/Kerosene*
Starting System	*Compressed Air*
Ignition System	*Spark Plug*
Lubrication	*6V pulsed oil pump*
Fuel Feed System	*12V turbine fuel pump*
Compressor	*Single stage centrifugal*
Thrust	*11 [lbf] at 123000 [RPM]*
Fuel consumption	*19.98 [lbm/hr]*
Throttle system	*Manual control*

Table A1.

THIS PAGE IS INTENTIONALLY LEFT BLANK

APPENDIX B. INSTRUMENTATION CALIBRATION RESULTS

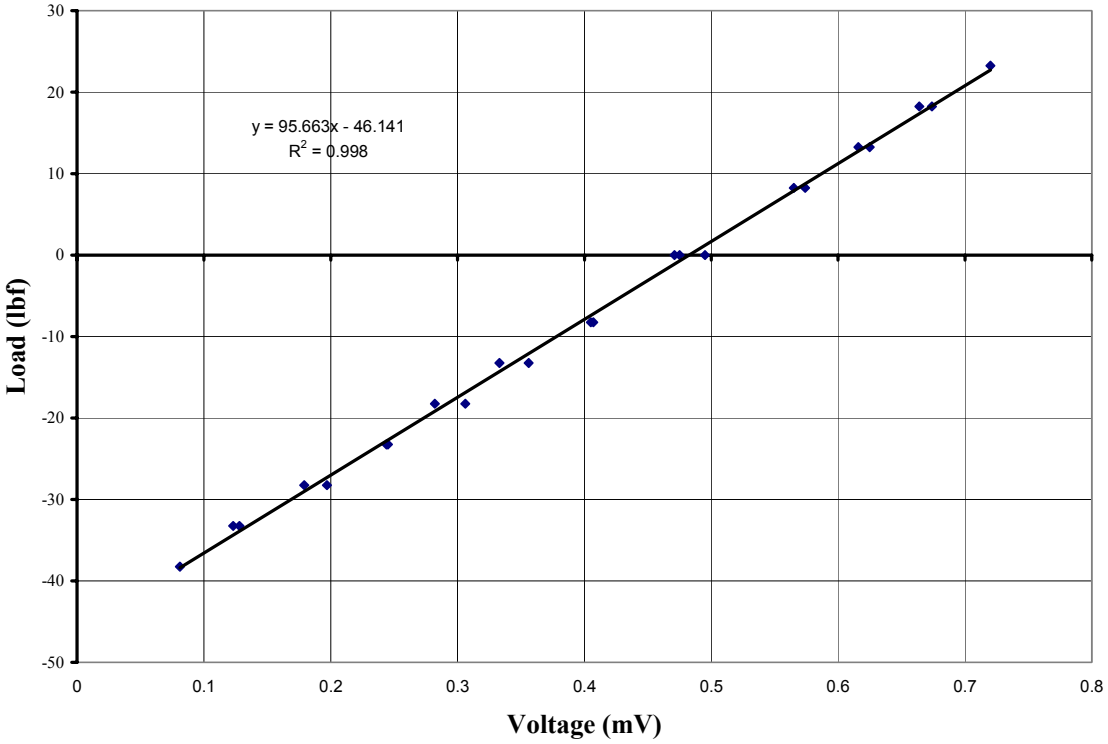

Figure 30. Thrust Beam Calibration

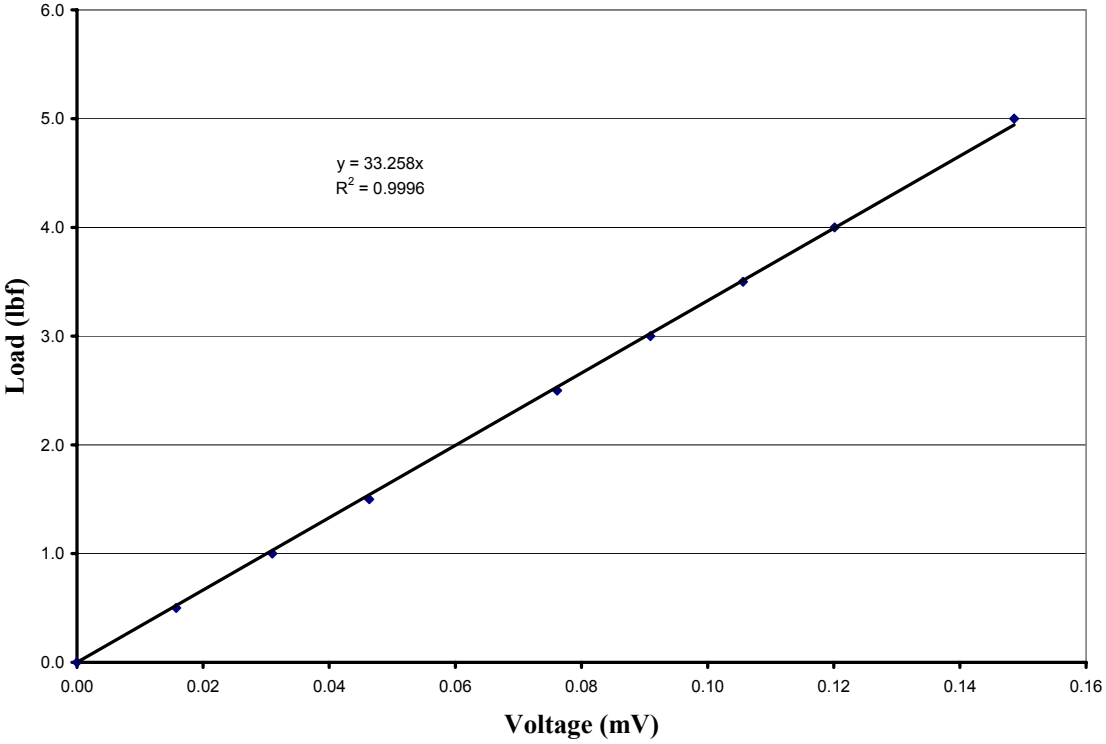

Figure 31. Fuel Flow Calibration

7 March 2003 Calibration Data			
Fuel		**Thrust**	
mV	**LBS**	**mV**	**LBS**
0.0000	0.0	0.475	0
0.0157	0.5	0.407	-8.25
0.0310	1.0	0.356	-13.25
0.0463	1.5	0.306	-18.25
0.0761	2.5	0.244	-23.25
0.0909	3.0	0.197	-28.25
0.1056	3.5	0.128	-33.25
0.1201	4.0	0.081	-38.25
0.1486	5.0	0.123	-33.25
		0.179	-28.25
		0.245	-23.25
		0.282	-18.25
		0.333	-13.25
		0.405	-8.25
		0.471	0
		0.565	8.25
		0.616	13.25
		0.664	18.25
		0.72	23.25
		0.674	18.25
		0.625	13.25
		0.574	8.25
		0.495	0

Table B1. Thrust and Fuel Flow Rate Calibration Values

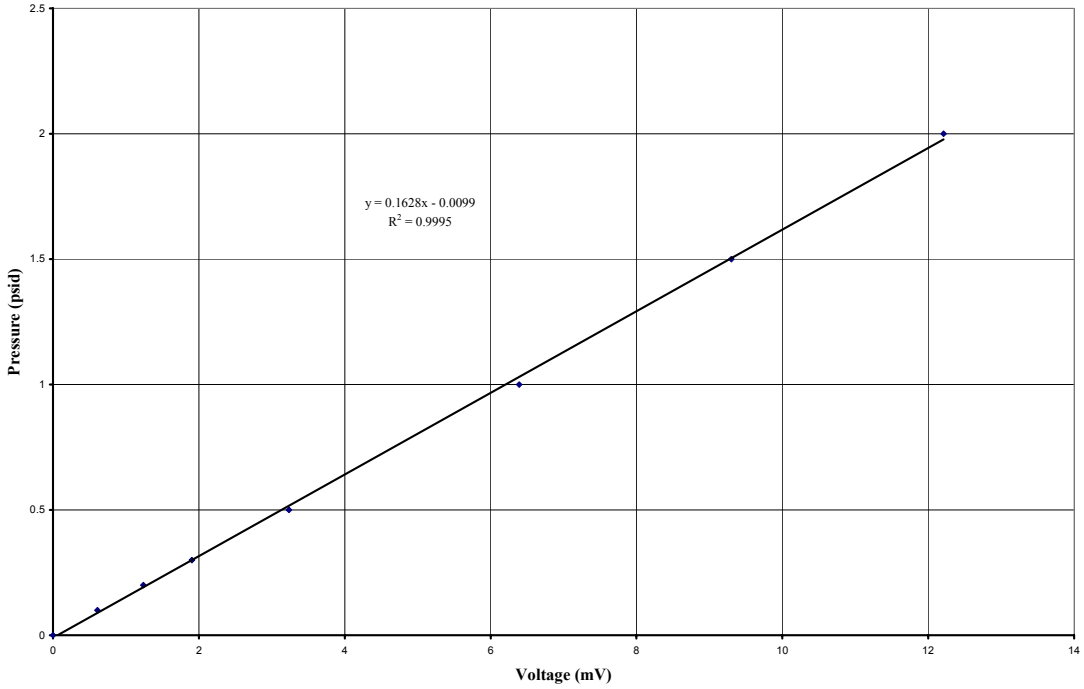

Figure 32. P1 Pressure Transducer Calibration.

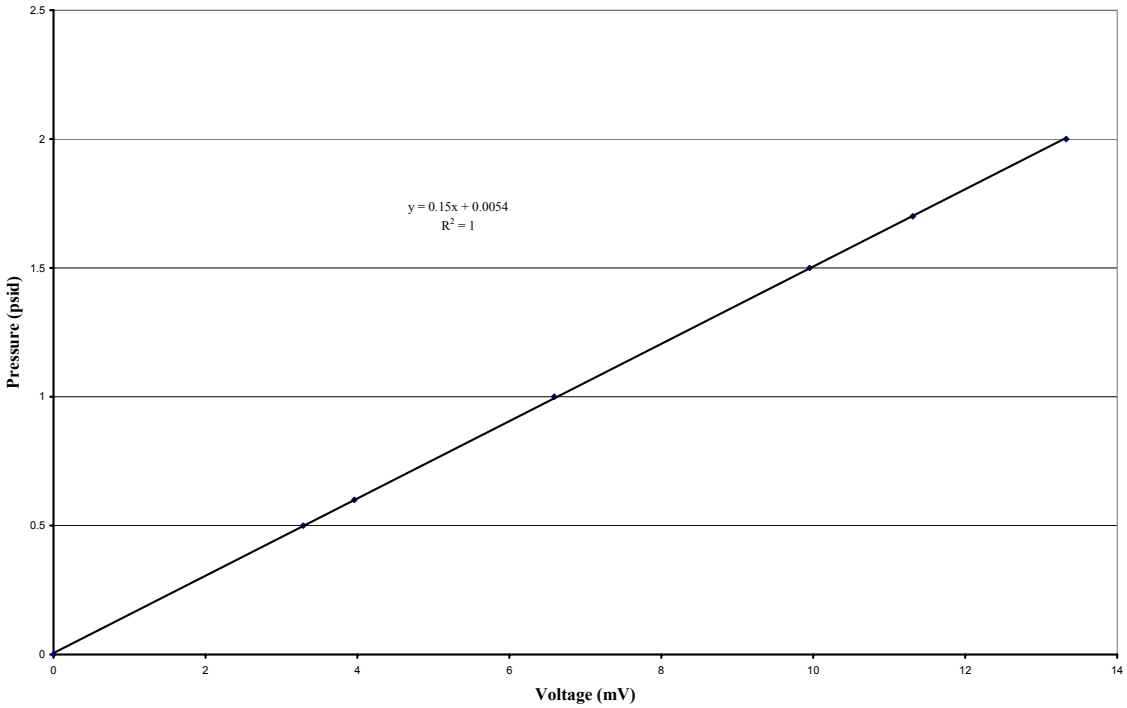

Figure 33. P2 Pressure Transducer Calibration

P 1	
MV	**psi**
12.21	2.0
9.30	1.5
6.39	1.0
3.23	0.5
1.90	0.3
1.24	0.2
0.61	0.1
0.00	0.0

Table B2. Pressure Transducer 1 Calibration Values

P 2	
MV	**psi**
13.33	2.0
11.31	1.7
9.95	1.5
6.59	1.0
3.96	0.6
3.29	0.5
0.00	0.0

Table B3. Pressure Transducer 2 Calibration Values

THIS PAGE IS INTENTIONALLY LEFT BLANK

APPENDIX C. SHROUDED ENGINE AT 100% SPOOL SPEED IN FREEJET FLOW RESULTS

26-Aug-02		
Mach No	Thrust (lbf)	Fuel Flow (lbm/sec)
0.5235	-35.23	NA
0.5062	-30.97	0.0043
0.4888	-27.92	0.0042
0.4721	-24.72	0.0043
0.4567	-23.43	0.0041
0.4387	-20.33	NA
0.4245	-18.28	0.0041
0.4112	-16.55	0.0041
0.3987	-14.83	0.0041
0.3865	-13.30	0.0042
0.3730	-11.88	NA
0.3622	-10.20	0.0040
0.3518	-9.22	0.0043
0.3418	-8.07	0.0043
0.3321	-7.18	0.0043
0.3209	-6.18	NA
0.3121	-5.31	0.0043
0.3034	-4.84	0.0043
0.2949	-3.89	0.0043
0.2866	-3.22	0.0040
0.2738	-2.25	NA
0.2661	-1.85	0.0043
0.2587	-1.08	0.0044
0.1931	1.56	0.0043

Table C1. Measurements of Single Thrust Beam Run at 100% Spool Speed

	P total (psig)	P1 (psig)	P2 (psig)	Fuel Flow (lbm/s)	Thrust (lbf)	Mach #
Run #1	0.0000	0.1193	0.0553	0.00415	10.56	0.000
	0.0000	0.1194	0.0599	0.00419	10.56	0.000
	0.0000	0.1173	0.0591	0.00401	10.47	0.000
	0.0000	0.1202	0.0583	0.00412	10.51	0.000
	0.0000	0.1191	0.0533	0.00413	10.42	0.000
	0.4676	0.1745	0.1614	0.00569	5.00	0.212
	0.4792	0.1741	0.1619	0.00564	4.30	0.214
	0.4724	0.1719	0.1568	0.00564	4.49	0.213
	0.4667	0.1668	0.1575	0.00564	4.51	0.212
	0.4617	0.1659	0.1526	0.00563	4.63	0.210
	0.4576	0.1626	0.1533	0.00554	4.89	0.209
	1.5233	0.7945	0.6382	0.00561	-10.57	0.378
	1.5563	0.8150	0.6428	0.00543	-12.40	0.381
	0.0062	0.1144	0.0544	0.00544	3.52	0.025
	0.0000	0.1170	0.0597	0.00572	7.73	0.000
	0.0000	0.1199	0.0561	0.00571	7.76	0.000
	0.0000	0.1185	0.0802	0.00568	7.87	0.000
	1.2751	0.6672	0.5489	0.00563	-6.98	0.346
	1.3568	0.6918	0.5519	0.00532	-9.81	0.357
	1.3388	0.6821	0.5424	0.00567	-8.93	0.355
	1.3247	0.6793	0.5396	0.00554	-9.18	0.353
	1.3080	0.6693	0.5287	0.00576	-9.38	0.351
	1.2990	0.6611	0.5313	0.00545	-9.37	0.349
	1.2878	0.6567	0.5249	0.00550	-9.09	0.348
	1.2723	0.6414	0.5158	0.00565	-9.04	0.346
	1.2635	0.6443	0.5114	0.00540	-8.92	0.345
	1.2459	0.6306	0.5038	0.00527	-8.93	0.342
	1.2315	0.6279	0.4976	0.00543	-9.02	0.341
	1.2097	0.6067	0.4835	0.00523	-8.79	0.338
	1.1920	0.5996	0.4829	0.00517	-8.46	0.335
	1.1662	0.5867	0.4721	0.00526	-8.28	0.332
	1.1475	0.5757	0.4663	0.00526	-8.02	0.329
	1.1441	0.5802	0.4610	0.00539	-7.81	0.329
	3.2658	2.0162	1.5759	0.00524	-39.72	0.542
	3.2704	2.0393	1.5598	0.00517	-49.54	0.543
	3.2696	1.9999	1.5322	0.00514	-48.91	0.543
	0.0000	0.1082	0.0536	0.00520	3.02	0.000
	0.0000	0.1076	0.0522	0.00553	3.77	0.000

Table C2. Measurements of Dual Thrust Beam Run 1 at 100% Spool Speed

	P total (psig)	P1 (psig)	P2 (psig)	Fuel Flow (lbm/s)	Thrust (lbf)	Mach #
Run #2	0.0000	0.1203	0.0526	0.00424	4.28	0.000
	0.0000	0.1229	0.0502	0.00446	4.22	0.000
	1.4647	0.7756	0.6001	0.00414	-13.84	0.370
	1.4564	0.7549	0.5923	0.00398	-14.26	0.369
	1.4477	0.7481	0.5885	0.00406	-14.09	0.368
	1.4392	0.7460	0.5865	0.00427	-13.91	0.367
	1.4003	0.7182	0.5675	0.00561	-13.79	0.362
	3.2741	2.2230	1.7370	0.00552	-47.07	0.543
	3.2755	2.2630	1.7451	0.00529	-51.77	0.543
	3.2748	2.2363	1.7122	0.00531	-51.70	0.543
	3.2748	2.2161	1.6990	0.00515	-51.29	0.543
	3.2732	2.2143	1.6840	0.00524	-50.58	0.543
	3.2731	2.1757	1.6495	0.00520	-50.17	0.543
	3.2719	2.1562	1.6347	0.00531	-49.41	0.543
	3.2716	2.1222	1.6100	0.00526	-48.98	0.543
	3.2707	2.0827	1.5797	0.00513	-47.97	0.543
	3.2656	1.9604	1.4920	0.00522	-45.29	0.542
	3.2630	1.8415	1.3882	0.00423	-44.09	0.542
	3.2560	1.7508	1.3255	0.00555	-41.63	0.542
	3.1251	1.6603	1.2521	0.00478	-39.51	0.531
	2.9619	1.5707	1.1870	0.00497	-37.40	0.518
	2.8149	1.4960	1.1317	0.00505	-35.69	0.506
	2.6770	1.4348	1.0932	0.00582	-31.94	0.494
	2.5368	1.3595	1.0456	0.00584	-30.39	0.482
	2.4180	1.2949	0.9956	0.00592	-28.83	0.471
	2.3032	1.2305	0.9466	0.00572	-27.20	0.460
	2.1915	1.1666	0.9044	0.00586	-25.89	0.449
	2.0949	1.1100	0.8610	0.00593	-24.78	0.440
	2.0129	1.0744	0.8340	0.00594	-23.59	0.432
	0.0000	0.1177	0.0447	0.00581	1.39	0.000
	0.0000	0.1184	0.0517	0.00589	3.67	0.000
	0.0000	0.1181	0.0449	0.00560	3.59	0.000

Table C3. Measurements of Dual Thrust Beam Run 2 at 100% Spool Speed

19 October 2000	
Mach #	**Thrust**
0.4100	-18.95
0.4000	-17.59
0.3900	-16.11
0.3700	-15.04
0.3600	-13.50
0.3500	-12.07
0.3500	-11.12
0.3400	-10.20
0.3300	-9.41
0.3200	-8.50
0.3100	-7.56
0.3000	-6.82
0.2965	-6.12
0.2898	-5.50
0.2829	-4.80
0.2761	-3.80
0.2693	-3.40
0.2622	-3.10
0.2549	-1.85
0.2489	-1.50
0.2426	-1.22
0.2326	-0.83
0.2296	-0.50
0.2239	0.09
0.2180	0.60
0.2119	0.99
0.2057	1.34
0.2010	1.70
0.1968	1.85
0.1925	2.20
0.1881	2.35
0.1836	2.68
0.1776	3.15
0.1715	3.33
0.1651	3.70
0.1584	3.89
0.1522	4.39
0.1390	4.68
0.1319	4.90

Table C4. Measurements of Garcia Run 2 at 100% Spool Speed (From: Ref 7)

APPENDIX D. SAMPLE MASS FLOW RATE CALCULATION AT M = 0.212

Measured Values from Table C2:

P_1=.1668 psi

P_{static}=14.736

Initially assume T_7 = 1000 deg R

Rearranging the perfect gas equation of state equation (13) $\rho = \frac{P}{RT}$,

$$\rho_7 = \frac{P}{RT} = \frac{(.1668 + 14.736)(144)}{53.34(1000)} = .04023 \text{ lbm/ft}^3$$

Using equation (9)

$$V_e = \sqrt{\frac{\frac{2}{\rho_7}\Delta P g_c}{\left[1 - \left(\frac{A_e}{A_1}\right)^2\right]}}$$

$$V_e = \sqrt{\frac{\frac{2}{.04023}.1668(144)(g_c)}{\left[1 - \left(\frac{.054463}{.110447}\right)^2\right]}} = 225.3 \text{ ft/s}$$

Then mass flow was calculated using equation (10)

$$\dot{m} = C_d \rho A V = .95(.04023)(.054463)(225.3) = .46896 \text{ lbm/s}$$

Equation (11) to determine total temperature

$$T_{t7} = \frac{\dot{m}_6 C_{p6} T_{t6} + \dot{m}_{6'} C_{p6'} T_{t6'}}{\dot{m} C_{p7}}$$

$$T_{t7} = \frac{(.271)(205.74)(1660) + (.19796)(186.69)(524.65)}{(.46896)(199.3274)} = 1197.57$$

Next equation (7)

$$V_7 = \frac{A_e V_e}{A_7} = 111.1 \text{ ft/s}$$

And equation (12)

$$T_7 = T_{t7} - \frac{\gamma_7 - 1}{2}\frac{V_7{}^2}{\gamma_7 R}$$

$$T_7 = 1197.57 - \frac{1.365 - 1}{2}\frac{111.1^2}{1.365(53.34)} = 1166.6 \text{ deg R}$$

The temperature for the second iteration was assumed to be 1324 deg R and the following values calculated.

$\rho = 0.03095$

$V_e = 256.88$

$\dot{m}_7 = 0.4113$

$T_{t7} = 1325.28$

$V_7 = 126.67$

$T_7 = 1324.03$

	P total	P1	Mach #	m6	TT6	rho 1	Ve1	m dot 1	tt7 1	t7 1
Run #1	0.0000	0.1193	0.000	0.260	1707	0.02351	249.27	0.3032	1706.90	1705.76
	0.0000	0.1194	0.000	0.260	1707	0.02351	249.37	0.3033	1706.90	1705.76
	0.0000	0.1173	0.000	0.260	1707	0.0235	247.18	0.3006	1706.90	1705.78
	0.0000	0.1202	0.000	0.260	1707	0.02351	250.15	0.3043	1706.90	1705.75
	0.0000	0.1191	0.000	0.260	1707	0.02351	249.03	0.3029	1706.90	1705.76
	0.4676	0.1745	0.212	0.271	1660	0.0308	263.40	0.4197	1308.8	1307.49
	0.4792	0.1741	0.214	0.271	1660	0.03075	263.29	0.4189	1310.44	1309.13
	0.4724	0.1719	0.213	0.271	1660	0.03096	260.71	0.4176	1312.93	1311.64
	0.4667	0.1668	0.212	0.271	1660	0.03095	256.88	0.4113	1325.28	1324.03
	0.4617	0.1659	0.210	0.271	1660	0.03095	256.19	0.4102	1327.52	1326.27
	0.4576	0.1626	0.209	0.271	1660	0.03024	256.59	0.4015	1345.41	1344.17
	1.5233	0.7945	0.378	0.297	1570	0.05241	430.80	1.1682	802.996	799.27
	1.5563	0.8150	0.381	0.297	1570	0.05281	434.68	1.1877	798.44	794.646
	0.0062	0.1144	0.025	0.260	1707	0.02499	236.68	0.3061	1604.76	1603.73
	0.0000	0.1170	0.000	0.260	1707	0.02528	238.03	0.3114	1585.93	1584.89
	0.0000	0.1199	0.000	0.260	1707	0.02564	239.28	0.3175	1565.02	1563.97
	0.0000	0.1185	0.000	0.260	1707	0.02548	238.58	0.3145	1575.08	1574.04
	1.2751	0.6672	0.346	0.292	1587	0.04998	404.28	1.0455	835.007	831.726
	1.3568	0.6918	0.357	0.292	1590	0.05042	409.84	1.0692	829.235	825.863
	1.3388	0.6821	0.355	0.292	1590	0.05021	407.84	1.0595	832.049	828.709
	1.3247	0.6793	0.353	0.292	1590	0.0502	407.03	1.0572	832.655	829.329
	1.3080	0.6693	0.351	0.292	1590	0.04999	404.89	1.0472	835.631	832.34
	1.2990	0.6611	0.349	0.292	1590	0.04978	403.23	1.0386	838.268	835.003
	1.2878	0.6567	0.348	0.291	1590	0.04977	401.94	1.0350	838.214	834.971
	1.2723	0.6414	0.346	0.291	1590	0.04942	398.61	1.0193	843.17	839.98
	1.2635	0.6443	0.345	0.291	1590	0.04949	399.23	1.0222	842.14	838.941
	1.2459	0.6306	0.342	0.291	1590	0.04921	396.09	1.0085	846.555	843.405
	1.2315	0.6279	0.341	0.291	1590	0.04914	395.50	1.0056	847.427	844.286
	1.2097	0.6067	0.338	0.287	1600	0.04873	390.43	0.9844	852.917	849.857
	1.1920	0.5996	0.335	0.287	1600	0.04859	388.69	0.9772	855.308	852.274
	1.1662	0.5867	0.332	0.287	1600	0.04827	385.77	0.9634	860.114	857.126
	1.1475	0.5757	0.329	0.287	1600	0.04801	383.17	0.9518	864.283	861.335
	1.1441	0.5802	0.329	0.287	1600	0.04808	384.38	0.9562	862.621	859.654
	3.2658	2.0162	0.542	0.338	1470	0.06602	611.46	2.0887	692.817	685.31
	3.2704	2.0393	0.543	0.338	1470	0.06621	614.08	2.1037	691.674	684.093
	3.2696	1.9999	0.543	0.338	1470	0.06586	609.72	2.0777	693.721	686.247
	0.0000	0.1082	0.000	0.260	1707	0.02349	237.50	0.2887	1706.9	1705.86
	0.0000	0.1076	0.000	0.260	1707	0.02349	236.83	0.2878	1706.9	1705.87

Table D1. Mass Flow Calculations Run 1

Run #2	P total	P1	Mach #	m6	TT6	rho 1	Ve1	m dot 1	tt7 1	t7 1
	0.0000	0.1203	0.000	0.260	1707	0.02351	250.30	0.3045	1706.9	1705.75
	0.0000	0.1229	0.000	0.260	1707	0.02351	252.92	0.3077	1706.9	1705.72
	1.4647	0.7756	0.370	0.296	1570	0.05221	426.44	1.1521	805.678	802.022
	1.4564	0.7549	0.369	0.296	1580	0.05163	423.10	1.1302	814.07	810.471
	1.4477	0.7481	0.368	0.296	1580	0.05148	421.81	1.1235	815.822	812.245
	1.4392	0.7460	0.367	0.296	1580	0.05141	421.50	1.1212	816.406	812.834
	1.4003	0.7182	0.362	0.294	1580	0.05107	414.94	1.0963	820.945	817.484
	3.2741	2.2230	0.543	0.338	1470	0.06733	635.79	2.2148	683.443	675.316
	3.2755	2.2630	0.543	0.338	1470	0.06819	637.43	2.2489	681.086	672.917
	3.2748	2.2363	0.543	0.338	1470	0.06798	634.62	2.2322	682.233	674.136
	3.2748	2.2161	0.543	0.338	1470	0.0678	632.60	2.2191	683.146	675.101
	3.2732	2.2143	0.543	0.338	1470	0.06779	632.37	2.2181	683.207	675.167
	3.2731	2.1757	0.543	0.338	1470	0.06744	628.49	2.1930	684.995	677.054
	3.2719	2.1562	0.543	0.338	1470	0.06726	626.48	2.1802	685.908	678.018
	3.2716	2.1222	0.543	0.338	1470	0.06693	623.07	2.1576	687.57	679.765
	3.2707	2.0827	0.543	0.338	1470	0.06658	618.87	2.1318	689.505	681.805
	3.2656	1.9604	0.542	0.338	1470	0.06542	605.71	2.0502	695.928	688.552
	3.2630	1.8415	0.542	0.338	1470	0.0643	592.14	1.9700	702.782	695.733
	3.2560	1.7508	0.542	0.337	1470	0.06349	581.03	1.9088	707.833	701.046
	3.1251	1.6603	0.531	0.335	1480	0.06261	569.80	1.8458	713.908	707.38
	2.9619	1.5707	0.518	0.328	1490	0.06192	557.30	1.7853	717.025	710.781
	2.8149	1.4960	0.506	0.327	1495	0.0612	547.05	1.7323	722.296	716.28
	2.6770	1.4348	0.494	0.325	1500	0.06063	538.26	1.6886	726.26	720.435
	2.5368	1.3595	0.482	0.318	1515	0.05993	526.98	1.6341	730.629	725.046
	2.4180	1.2949	0.471	0.317	1515	0.05928	517.12	1.5862	735.464	730.088
	2.3032	1.2305	0.460	0.315	1525	0.05849	507.53	1.5358	742.504	737.325
	2.1915	1.1666	0.449	0.313	1526	0.05778	497.18	1.4864	747.928	742.959
	2.0949	1.1100	0.440	0.311	1530	0.05711	487.79	1.4415	753.825	749.041
	2.0129	1.0744	0.432	0.309	1530	0.05676	481.41	1.4138	756.346	751.686
	0.0000	0.1177	0.000	0.260	1707	0.02538	238.25	0.3129	1580.78	1579.73
	0.0000	0.1184	0.000	0.260	1707	0.02548	238.56	0.3145	1575.19	1574.14
	0.0000	0.1181	0.000	0.260	1707	0.02544	238.40	0.3139	1577.3	1576.26

Table D2. Mass Flow Calculations Run 2

APPENDIX E. AFTERBURNER MEASUREMENTS

	P total	P1	P2	FF	Thrust	Mach
Run #1	0.0000	0.0737	0.0532	NA	5.03	0.000
	0.0000	0.0742	0.0553	0.00329	5.22	0.000
	0.0000	0.0753	0.0555	NA	5.37	0.000
	0.0000	0.0759	0.0565	0.00404	5.53	0.000
	0.0000	0.0768	0.0581	0.00361	5.57	0.000
	0.0000	0.0777	0.0573	0.00377	5.68	0.000
	0.0000	0.0395	0.0222	0.00504	5.86	0.000
	0.0000	0.0181	0.0148	0.00623	5.74	0.000
	0.0000	0.0147	0.0084	0.00528	5.31	0.000
	0.0000	0.0126	0.0063	0.00483	5.04	0.000
	0.0000	0.0109	0.0031	0.00483	4.75	0.000
	0.0000	0.0080	0.0023	0.00491	4.70	0.000
	0.2219	0.0918	0.0897	0.00459	3.31	0.146
	0.2205	0.0886	0.1026	0.00474	3.51	0.146
	0.2188	0.1467	0.1471	0.00465	3.69	0.145
	0.2162	0.1453	0.1453	0.00471	3.75	0.144
	0.2159	0.1425	0.1397	0.04723	3.80	0.144
	0.2123	0.1366	0.1403	0.00501	3.82	0.143
	0.2077	0.1373	0.1315	0.00473	3.94	0.142
	0.3861	0.1710	0.1799	0.00513	1.28	0.193
	0.3804	0.1615	0.1786	0.00528	1.33	0.191
	0.3743	0.1604	0.1695	0.00541	1.47	0.190
	0.3704	0.1480	0.1611	0.00502	1.59	0.189
	0.3560	0.1389	0.1528	0.00500	1.70	0.185
	0.3510	0.1376	0.1477	0.00552	1.91	0.184
	0.3383	0.1301	0.1401	0.00509	2.01	0.180
	0.3340	0.1184	0.1369	0.00460	2.08	0.179
	0.3256	0.1188	0.1394	0.00471	2.17	0.177
	0.3207	0.1160	0.1301	0.00520	2.17	0.176
	0.2714	0.0830	0.1040	0.00498	2.59	0.162
	0.1446	0.0357	0.0662	0.00501	4.01	0.118

Table E1. Measurements of Afterburner Run 1.

Run # 2	P total	P1	P2	FF	Thrust	Mach
	0.0000	0.0715	0.0532	NA	5.08	0.000
	0.0000	0.0743	0.0551	0.00313	5.33	0.000
	0.0000	0.0763	0.0565	0.00339	5.44	0.000
	0.0000	0.0777	0.0580	0.00319	5.53	0.000
	0.0000	0.0777	0.0586	0.00281	5.65	0.000
	0.0000	0.0774	0.0521	0.00342	5.65	0.000
	0.0000	0.0556	0.0405	0.00290	5.82	0.000
	0.0000	0.0447	0.0311	0.00486	5.82	0.000
	0.0000	0.0285	0.0166	0.00489	5.87	0.000
	0.0000	0.0186	0.0119	0.00538	5.72	0.000
	0.0000	0.0165	0.0083	0.00525	5.60	0.000
	0.0000	0.0117	0.0055	0.00467	5.39	0.000
	0.0000	0.0088	0.0056	0.00508	5.33	0.000
	0.0000	0.0098	0.0048	0.00502	5.17	0.000
	0.0000	0.0123	0.0068	0.00503	5.29	0.000
	0.0000	0.0107	0.0072	0.00512	5.37	0.000
	0.0000	0.0131	0.0064	0.00469	5.41	0.000
	0.1533	0.0124	0.0243	0.00459	4.94	0.122
	0.1521	0.0591	0.0683	0.00556	4.26	0.121
	0.2786	0.1713	0.1721	0.00505	3.47	0.164
	0.2720	0.1702	0.1708	0.00463	3.50	0.162
	0.2365	0.1486	0.1464	0.00518	3.98	0.151
	0.2344	0.1549	0.1485	0.00507	4.00	0.150
	0.2301	0.1527	0.1558	0.00493	4.11	0.149
	0.2245	0.1488	0.1483	0.00509	4.31	0.147
	0.2228	0.1433	0.1433	0.00492	4.38	0.147
	0.3054	0.1275	0.1331	0.00416	3.29	0.171
	0.3017	0.1226	0.1310	NA	3.40	0.170
	0.2959	0.1098	0.1216	0.00494	3.48	0.169
	0.2869	0.1008	0.1232	0.00498	3.61	0.166
	0.1636	0.0964	0.0916	0.00632	4.72	0.126
	0.1601	0.0898	0.0900	0.00521	4.41	0.124
	0.1554	0.0888	0.0886	0.00482	4.33	0.122
	0.1501	0.0845	0.0843	0.00579	4.51	0.120
	0.1477	0.0831	0.0843	0.00513	4.80	0.119
	0.1446	0.0817	0.0815	0.00536	5.08	0.118
	0.1443	0.0793	0.0807	0.00553	5.24	0.118
	0.1421	0.0785	0.0816	0.00524	5.41	0.117

Table E2. Measurements of Afterburner Run 2.

Mach No	lbf
0.1962	-2.13
0.1869	-1.88
0.1770	-1.49
0.1666	-1.11
0.1554	-0.675
0.2436	-5.35
0.2397	-5.04
0.2358	-4.83
0.2317	-4.61
0.2276	-4.45
0.2378	-5.08
0.2373	-5.15
0.2368	-5.28
0.2363	-5.12
0.2358	-5.05

Table E3. Results from Garcia (Ref 7) Shrouded Engine in Freejet at 80% Spool Speed

THIS PAGE IS INTENTIONALLY LEFT BLANK

APPENDIX F. RESULTS AND INPUT FILES TO OVERFLOW

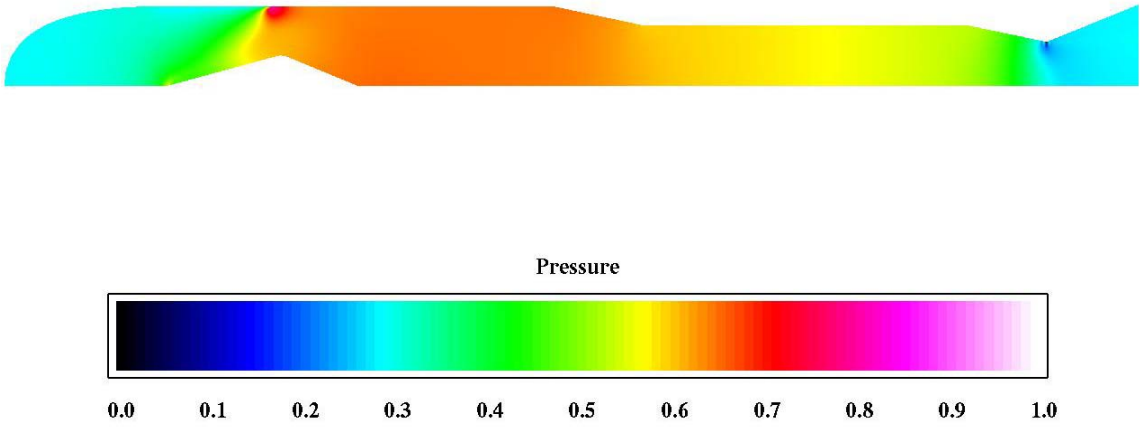

Figure 34. Pressure Distribution for Turbo-Ramjet Shroud at M_∞=0.6

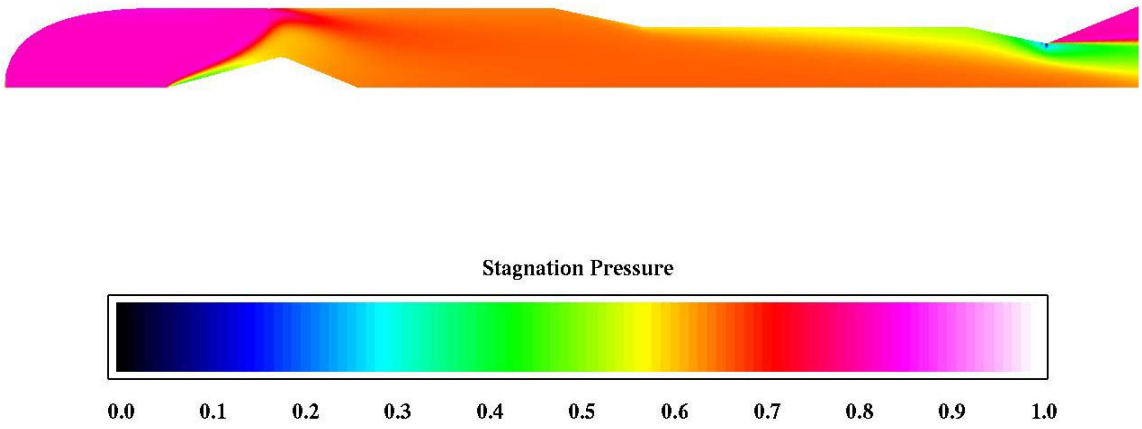

Figure 35. Stagnation Pressure Distribution for Turbo-Ramjet Shroud at M_∞=0.6

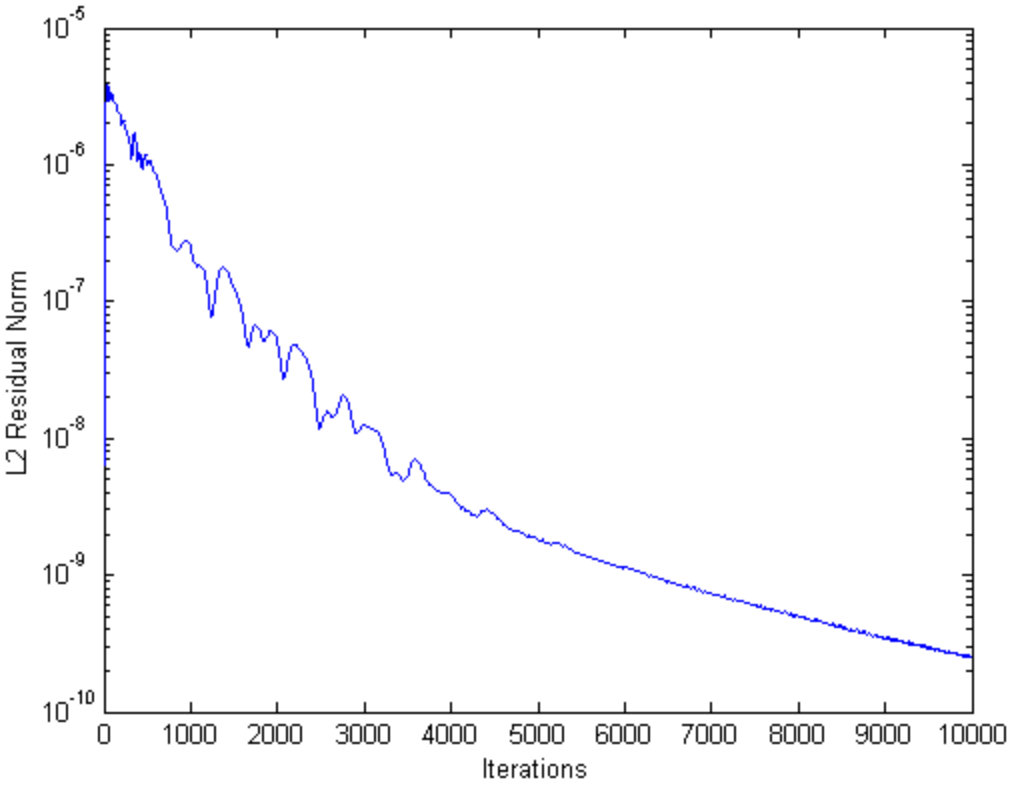

Figure 36. L2 Residual Norm for Turbo-Ramjet Shroud at M_∞=0.6

Overflow.in Input File for Turbo-Ramjet Shroud

```
$GLOBAL
     CHIMRA= .F.,   NSTEPS=10000,   RESTRT= .F.,   NSAVE =100,
     NQT   = 202,
     $END
 $FLOINP
     ALPHA =0,  FSMACH= .6000,  REY   = 1.1420E7,  TINF  = 520.000,
     XKINF=.0001, RETINF=0.1, GAMINF=1.4,
     $END
 $VARGAM
     IGAM=0,
     $END
 $GRDNAM
     NAME = 'Axi-symmetric shroud with nose cone',
 $END
 $NITERS
     $END
 $METPRM
     $END
 $TIMACU
     ITIME=1,
     CFLMIN=5,
     CFLMAX=10;
     $END
 $SMOACU
     $END
 $VISINP
     VISC =.T.,
     CFLT = 1,
     ITERT = 3,
     $END
 $BCINP
     NBC   =   9,
     IBTYP =   5,  5, 32, 32, 32, 22, 16,16, 16,
     IBDIR =  -2,  2,  1,  2, -2,  3,  1, 2,  2,
     JBCS  =  85, 31, -1,378,  1,  1,  1, 1,134,
     JBCE  = 377,133, -1, -1, 84, -1,  1,31, -1,
     KBCS  =  51,  1,  1, -1, -1,  1,  1, 1,  1,
     KBCE  =  51,  1, -1, -1, -1, -1, -1, 1,  1,
     LBCS  =   1,  1,  1,  1,  1,  1,  1, 1,  1,
     LBCE  =  -1, -1, -1, -1, -1,  1, -1,-1, -1,
 $END
 $SCEINP
 $END
```

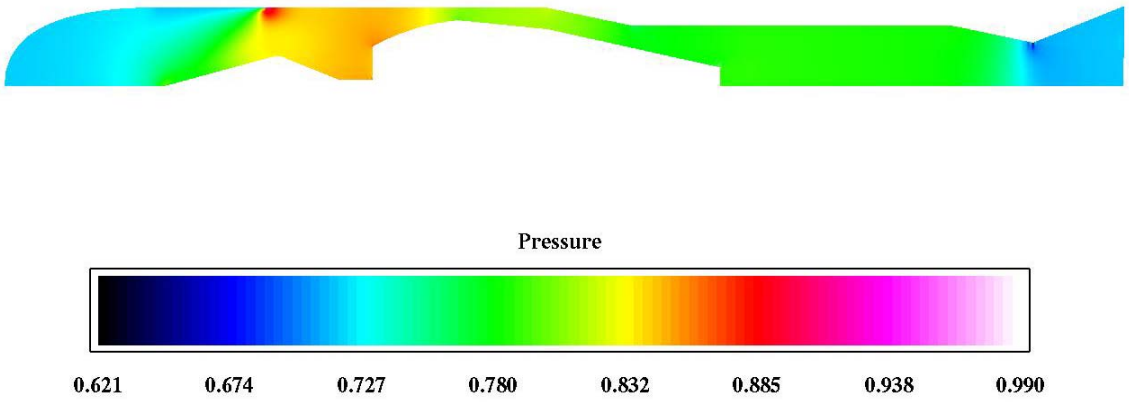

Figure 37. Pressure Distribution for Turbo-Ramjet with Engine Inflow/Outflow at M_∞=0.6

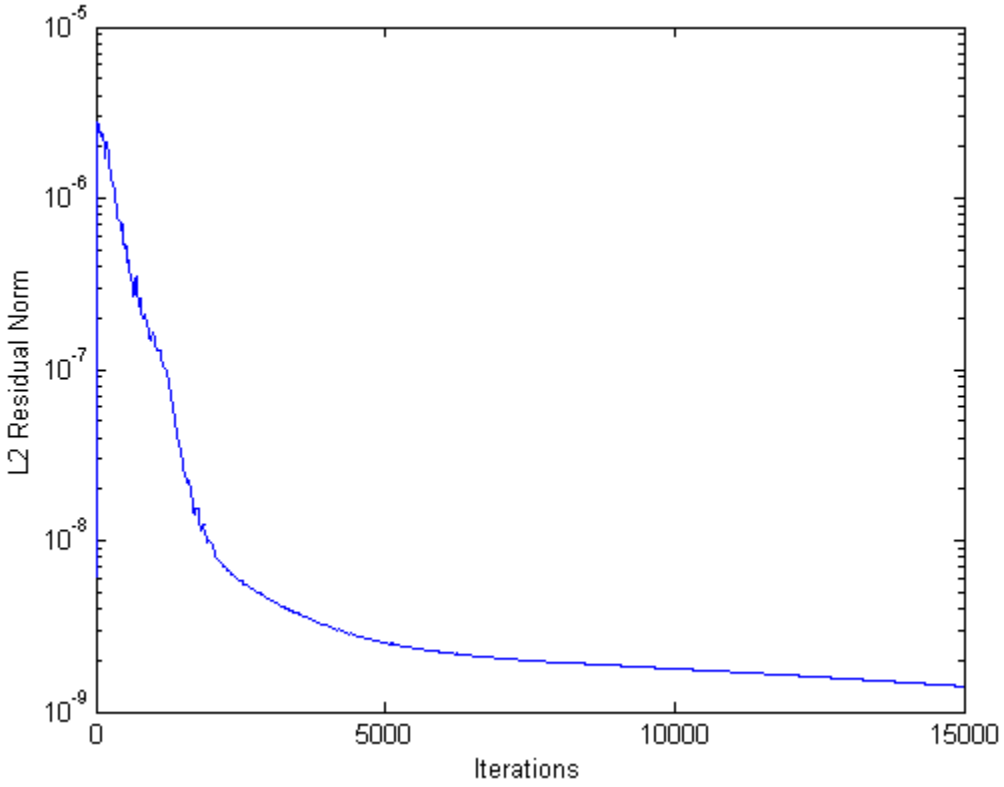

Figure 38. L2 Residual Norm for Turbo-Ramjet with Engine Inflow/Outflow at M_∞=0.6

Overflow.in Input File for Actual Turbo-Ramjet with Engine Inflow/Outflow

```
$GLOBAL
     CHIMRA= .F.,   NSTEPS=15000,   RESTRT= .F.,   NSAVE =100,
     NQT   = 202,
     $END
 $FLOINP
     ALPHA =0,  FSMACH= .6000,  REY   = 1.0420E7,  TINF  = 520.000,
     XKINF=.0001, RETINF=0.1, GAMINF=1.4,
     $END
 $VARGAM
     IGAM=0,
     $END
 $GRDNAM
     NAME = 'Axi-symmetric nozzle inlet',
 $END
 $NITERS
     $END
 $METPRM
     $END
 $TIMACU
     ITIME=1,
     CFLMIN=5,
     CFLMAX=10;
     $END
 $SMOACU
     $END
 $VISINP
     VISC =.T.,
     CFLT = 1,
     ITERT = 3,
     $END
 $BCINP
     NBC   =  12,
     IBTYP =   5,  5,  5, 32, 32, 32, 33, 49, 22, 16,16, 16,
     IBDIR =   2, -2,  2,  1,  2, -2, -2,  2,  3,  1, 2,  2,
     JBCS  =  31, 85,171, -1,523,  1,148,411,  1,  1, 1,429,
     JBCE  = 147,522,410, -1, -1, 84,170,428, -1,  1,30, -1,
     KBCS  =   1, -1,  1,  1, -1, -1,  1,  1,  1,  1, 1,  1,
     KBCE  =   1, -1,  1, -1, -1, -1,  1,  1, -1, -1, 1,  1,
     LBCS  =   1,  1,  1,  1,  1,  1,  1,  1,  1,  1, 1,  1,
     LBCE  =  -1, -1, -1, -1, -1, -1, -1, -1,  1, -1,-1, -1,
     BCPAR1(7)=1.18,
 $END
 $SCEINP
 $END
```

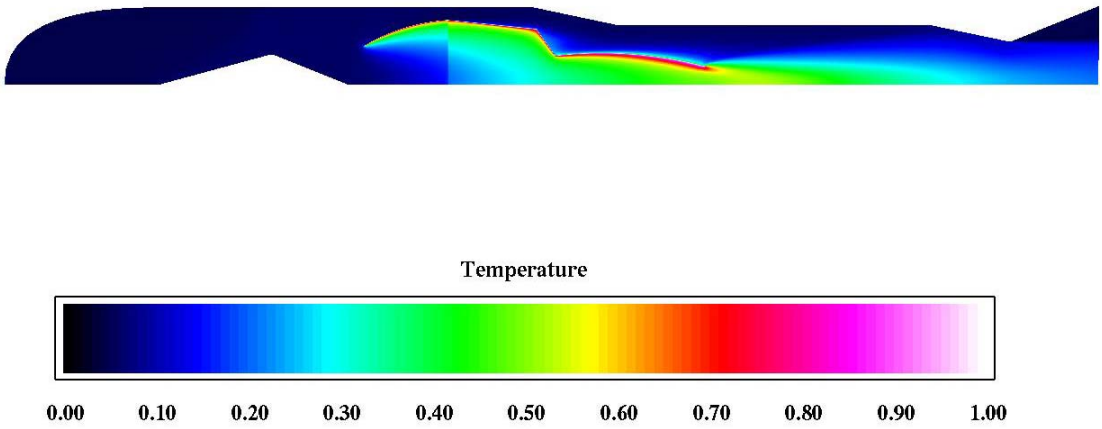

Figure 39. Temperature Distribution for Turbo-Ramjet with Engine Through Flow at M_∞=0.6

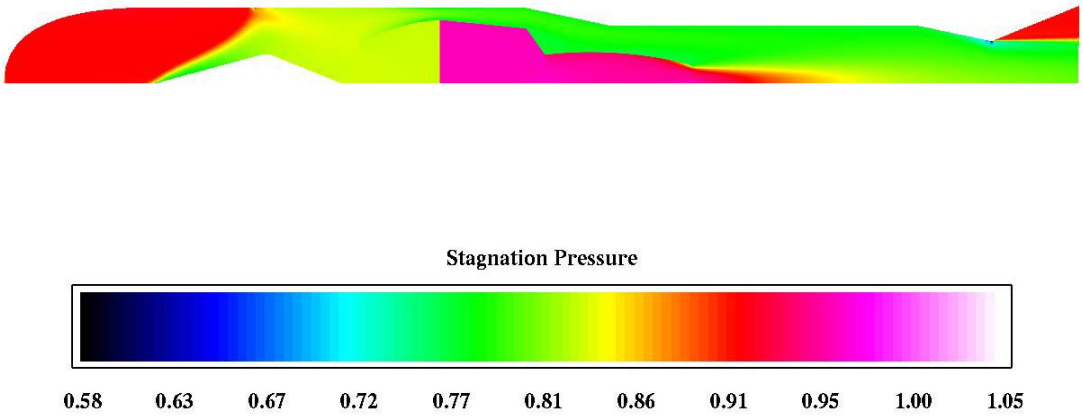

Figure 40. Stagnation Pressure Distribution for Turbo-Ramjet with Engine Through Flow at M_∞=0.6

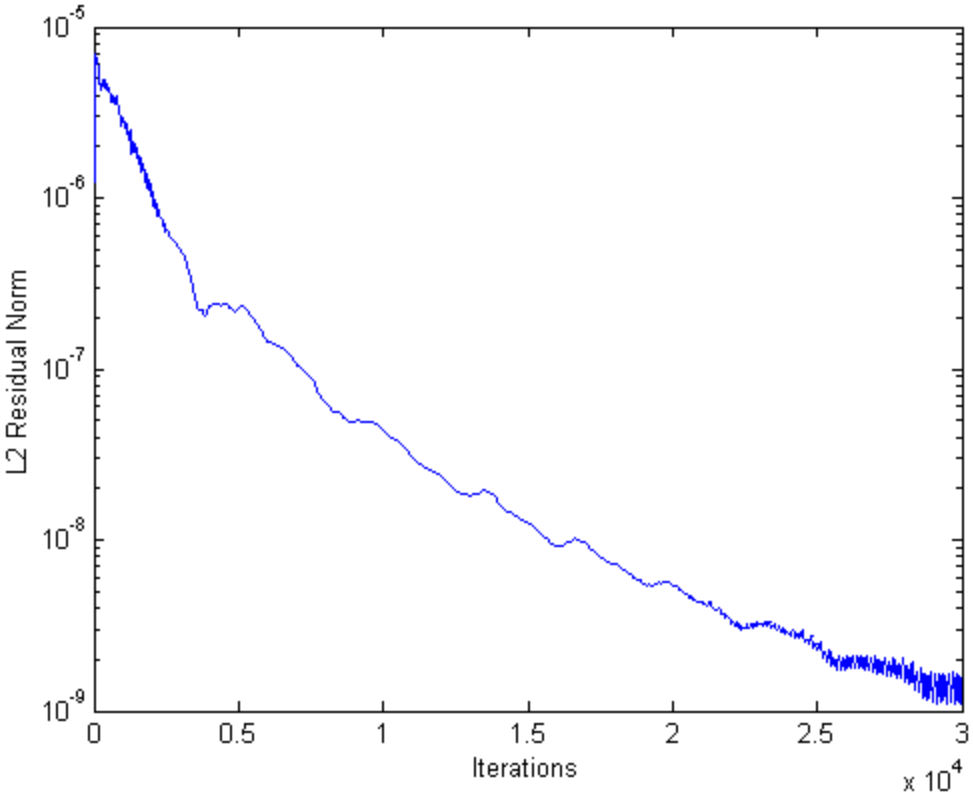

Figure 41. L2 Residual Norm for Turbo-Ramjet with Engine Through Flow at M_∞=0.6

Overflow.in Input File for Actual Turbo-Ramjet Through Flow Modeling

```
$GLOBAL
     CHIMRA= .F.,   NSTEPS=30000,   RESTRT= .F.,   NSAVE =1000,
     NQT   = 202,
     $END
 $FLOINP
     ALPHA =0,  FSMACH= .6000,  REY   = 1.0420E7,  TINF  = 520.000,
     XKINF=.0001, RETINF=0.1, GAMINF=1.4,
     $END
 $VARGAM
     IGAM=0,
     $END
 $GRDNAM
     NAME = 'Throughflow into engine heating grid TEMP change',
 $END
 $NITERS
     $END
 $METPRM
     $END
 $TIMACU
     ITIME=1,
     CFLMIN=1,
     CFLMAX=10;
     $END
 $SMOACU
     $END
 $VISINP
     VISC =.T.,
     CFLT = 1,
     ITERT = 3,
     $END
 $BCINP
     NBC   =  13,
     IBTYP =   5,  5,  5,  7,  7,  7, 44, 32, 32, 32, 22, 16, 16,
     IBDIR =   2, -2,  2,  2,  2, -2,  1,  2, -2,  1,  3,  1,  2,
     JBCS  =   1,105,191,296,382,191,290,558,  1, -1,  1,  1,173,
     JBCE  = 172,558,295,381,437,437,291, -1,104, -1, -1,  1, -1,
     KBCS  =   1, -1, 49, 49, 49, 48,  1, -1, -1,  1,  1,  1,  1,
     KBCE  =   1, -1, 49, 49, 49, 48, 47, -1, -1, -1, -1, -1,  1,
     LBCS  =   1,  1,  1,  1,  1,  1,  1,  1,  1,  1,  1,  1,  1,
     LBCE  =  -1, -1, -1, -1, -1, -1, -1, -1, -1, -1,  1, -1, -1,
     BCPAR1(4)=1000,
     BCPAR1(5)=1500,
     BCPAR1(6)=3000,
     BCPAR1(7)=.18,
 $END
 $SCEINP
 $END
```

APPENDIX G. PREDICTED RESULTS FROM GASTURB

Mach	Net Thrust	TT6	Pt6	Mdot 6
0.00	9.90	1706.90	19.135	0.260
0.05	9.49	1703.93	19.149	0.261
0.10	9.12	1695.01	19.191	0.263
0.15	8.80	1680.86	19.263	0.266
0.20	8.52	1661.79	19.365	0.270
0.25	8.28	1638.63	19.501	0.276
0.30	8.10	1614.09	19.684	0.283
0.35	7.95	1586.75	19.907	0.292
0.40	7.84	1557.58	20.173	0.302
0.45	7.75	1526.70	20.483	0.313
0.50	7.69	1496.31	20.838	0.326
0.55	7.65	1466.72	21.250	0.339
0.60	7.64	1438.16	21.727	0.355

Table G1. Predicted Off-Design Values of J450 Turbojet

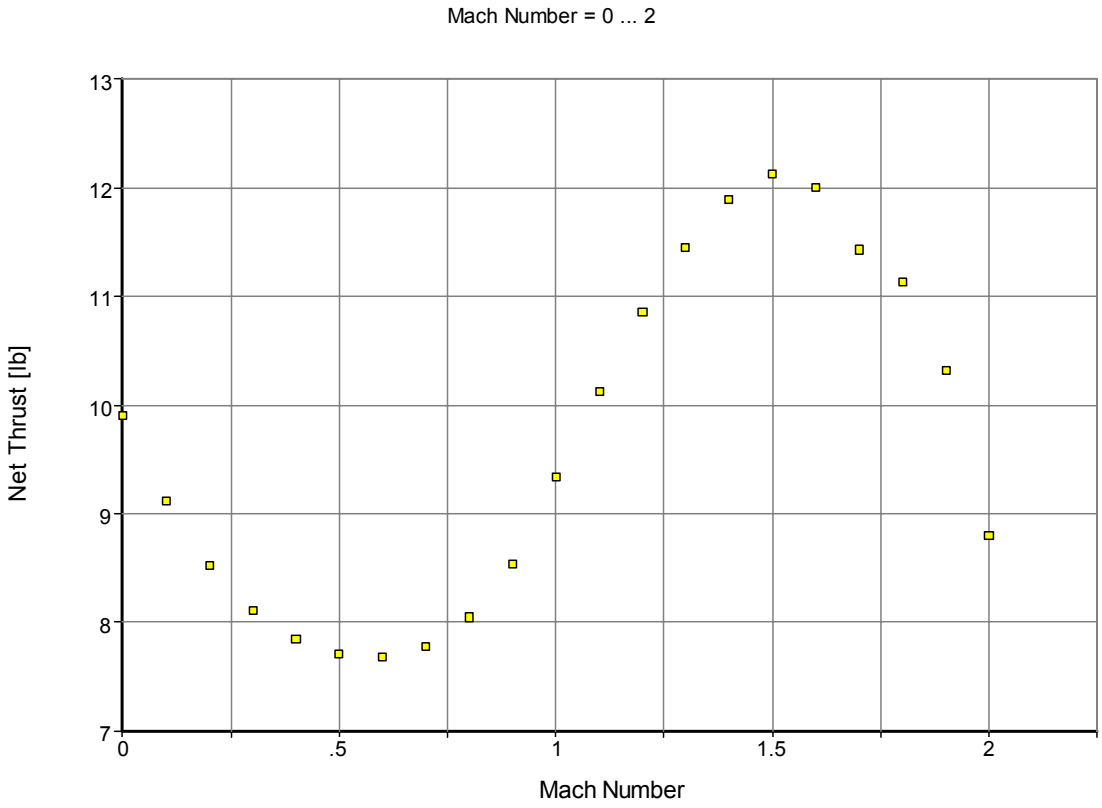

Figure 42. Predicted J450 Turbojet Net Thrust vs. Mach Number

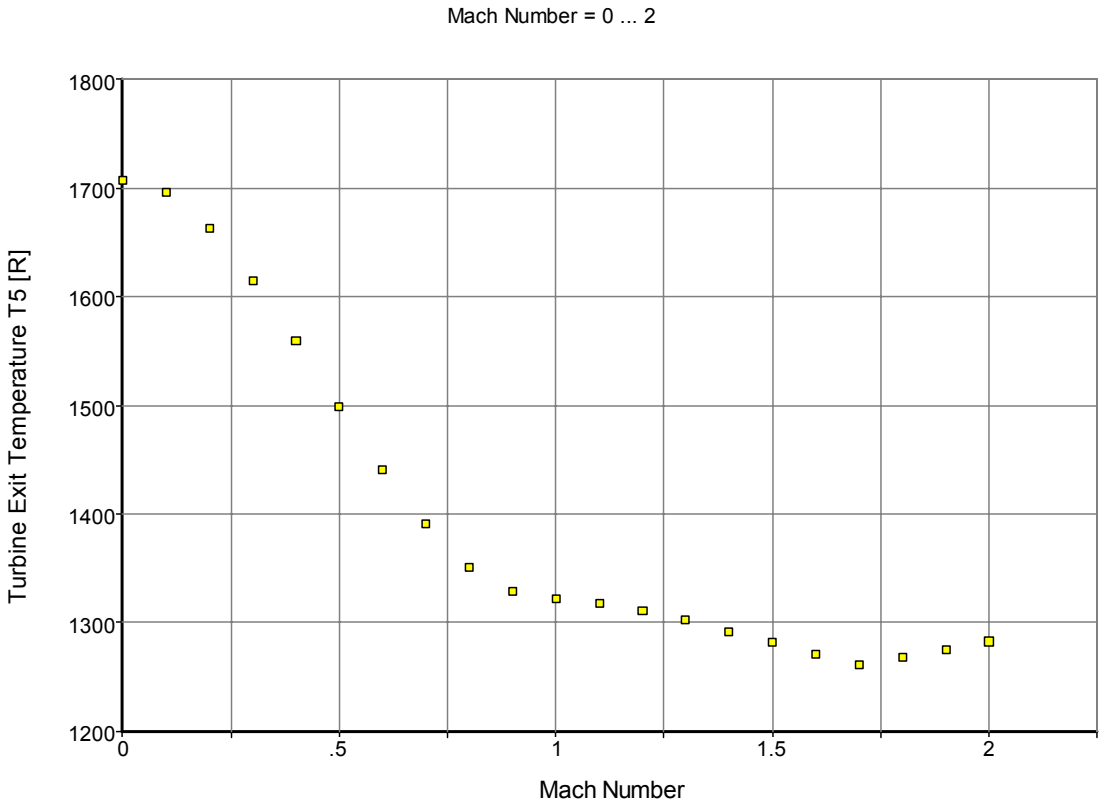

Figure 43. Predicted J450 Turbojet Turbine Exit Temperature vs. Mach Number

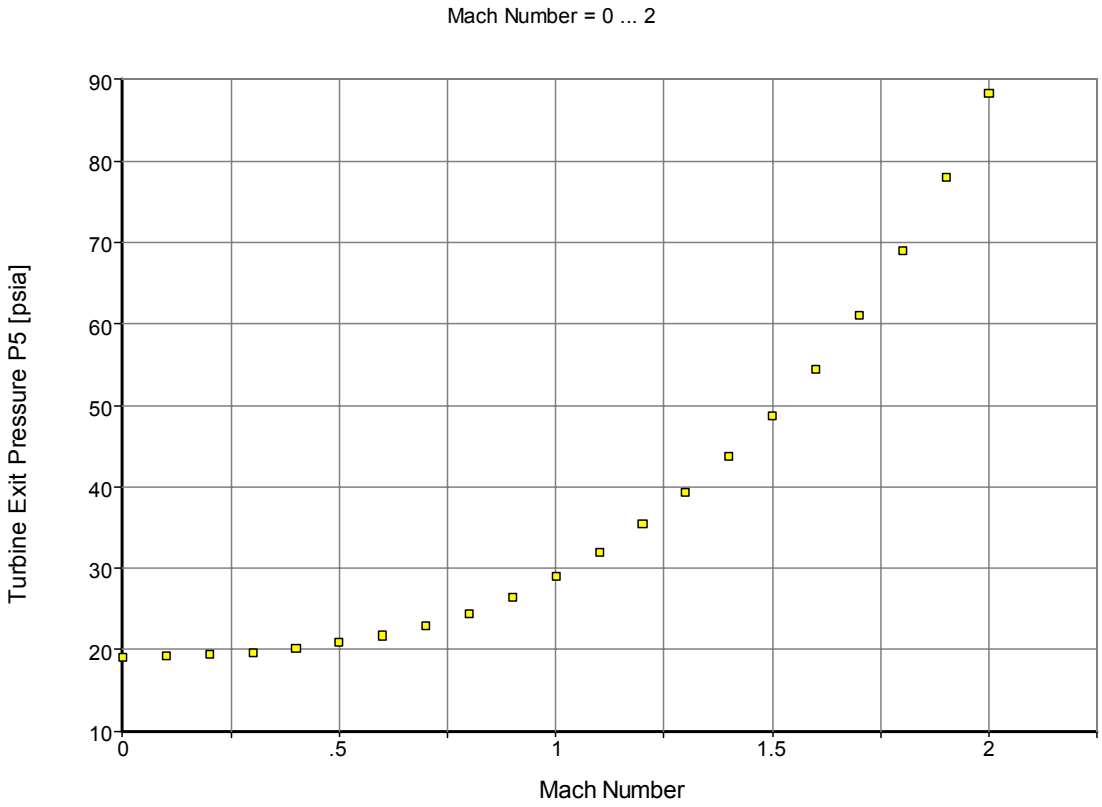

Figure 44. Predicted J450 Turbojet Turbine Exit Pressure vs. Mach Number

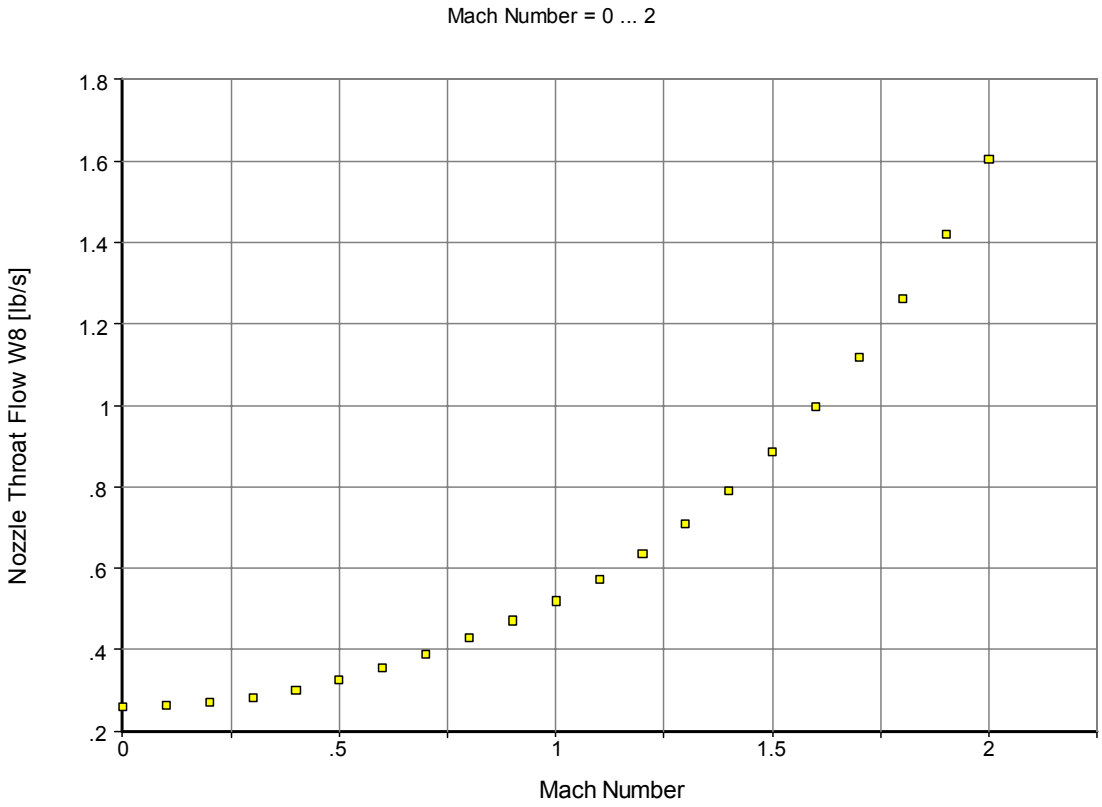

Figure 45. Predicted J450 Turbojet Mass Flow Rate vs. Mach Number

File: H:\thesis.CYM - modified
Date: Mar3103
Time: 21:54

mixed Turbofan SL Mn=0.200 ISA

Station	W	T	P	WRstd		
amb		518.67	14.696		FN	= 4.00
2	0.399	522.83	15.112	0.390	TSFC	= 8.0394
13	0.124	522.84	15.113		WF Burner	= 0.00400
21	0.275	522.84	15.113	0.269	s NOx	= 0.0425
25	0.275	522.84	15.113	0.269	BPR	= 0.4500
3	0.267	702.29	32.493	0.141	Core Eff	= 0.0764
31	0.238	702.29	32.493		Prop Eff	= 0.5887
4	0.242	1860.00	31.518	0.214	P3/P2	= 2.150
41	0.256	1803.10	31.518	0.223	P16/P6	= 0.81061
43	0.256	1637.22	18.443		A63	= 1.47
44	0.270	1592.81	18.443		A163	= 3.65
45	0.270	1592.81	18.074	0.384	A64	= 5.12
49	0.270	1592.79	18.073		XM63	= 0.56984
5	0.278	1566.12	18.073	0.393	XM163	= 0.05661
6	0.278	1566.12	17.712		XM64	= 0.20001
16	0.124	522.84	14.357		P63/P6	= 0.99000
64	0.396	1273.04	15.597		P163/P16	= 0.99000
7	0.182	2000.00	15.332		WF total	= 0.00893
8	0.407	1980.00	15.332	0.762	A8	= 6.07
P2/P1 = 1.0000		P6/P5 = 0.9800		CD8 = 0.8919	Ang8	= 16.43
Efficiencies:		isentr	polytr	RNI P/P	P8/Pamb	= 1.04327
Outer LPC		1.0000	0.9949	1.015 1.000	P16/P13	= 0.95000
Inner LPC		1.0000	0.9949	1.015 1.000	W_NGV/W25	= 0.05000
HP Compressor		0.7100	0.7391	1.015 2.150	WHcl/W25	= 0.05000
Burner		0.9995		0.970	Loading %	= 100.00
HP Turbine		0.7400	0.7268	0.266 1.709	WLcl/W25	= 0.03000
LP Turbine		1.0000	1.0000	0.187 1.000	WBLD/W21	= 0.00000
Mixer		1.0000			WBLD/W25	= 0.00500
HP Spool mech		1.0000	Nominal Spd	115000	PWX	= 0.0
LP Spool mech		1.0000	Nominal Spd	115000	ZWBld	= 0.00000
Reheat		0.9000		0.005	WF Reheat	= 0.98299
					XM64	= 0.20001
					XM7	= 0.26703

Fuel	FHV	humidity	war2
Generic	18552.4	0.0	0.0000

Table G2. Single Cycle Results of Turbo-Ramjet Modeled as Mixed Flow Turbofan

File: H:\thesis\thesis.CYM - modified
Date: Mar3103
Time: 22:00

mixed Turbofan SL Mn=0.200 ISA

Altitude	ft	0
Delta T from ISA	R	0
Relative Humidity [%]		0
Mach Number		0.2
Basic Data		
Intake Pressure Ratio		-1
Inner Fan Pressure Ratio		1
Booster Map Type (0/1/2)		0
Outer Fan Pressure Ratio		1
Compr. Interduct Press. Ratio		1
HP Compressor Pressure Ratio		2.15
Bypass Duct Pressure Ratio		0.95
Turb. Interd. Ref. Press. Ratio		0.98
Design Bypass Ratio		0.45
Burner Exit Temperature	R	1860
Burner Design Efficiency		0.9995
Burner Partload Constant		1.6
Fuel Heating Value	BTU/lb	18552.4
Handling Bleed Location		0
Overboard Bleed	lb/s	0
Power Offtake	hp	0
HP Spool Mechanical Efficiency		1
LP Spool Mechanical Efficiency		1
Burner Pressure Ratio		0.97
Turbine Exit Duct Press Ratio		0.98
Hot Stream Mixer Press Ratio		0.99
Cold Stream Mixer Press Ratio		0.99
Mixed Stream Pressure Ratio		1
Mixer Efficiency		0.5
Design Mixer Mach Number		0.2
Design Mixer Area	in²	0
Nozzle Thrust Coefficient		1
Design Nozzle Petal Angle [°]		25
Air System		
Rel. Handling Bleed to Bypass		0
Rel. Enthalpy of HP Handl.Bleed		0
Rel. HP Leakage to Bypass		0
Rel. Overboard Bleed W_Bld/W25		0.005
Rel. Enthalpy of Overb. Bleed		1
NGV Cooling Air W_Cl_NGV/W25		0.05
LPT Cooling Air W_Cl/W25		0.03
Rel. Enth. of LPT Cooling Air		0.6
HPT Cooling Air W_Cl/W25		0.05
Rel.HP Leakage to LPT exit		0
Rel. Fan Overb.Bleed W_Bld/W13		0
Mass Flow Input		
Inlet Corr. Flow W2Rstd	lb/s	0.39
LPC Efficiency		
Isentr.Inner LPC Efficiency		1
Isentr.Outer LPC Efficiency		1

Table G3. Input Table for GASTURB Turbofan Modeling of Turbo-Ramjet

LPC Design		
Nominal LP Spool Speed		115000
HPC Efficiency		
Isentr. HPC Efficiency		0.71
HPC Design		
Nominal HP Spool Speed		115000
HPT Efficiency		
Isentr. HPT Efficiency		0.74
LPT Efficiency		
Isentr. LPT Efficiency		1
Reheat Selection		
Reheat Exit Temperature	R	2000
Reheat Design Efficiency		0.9
Reheat Partload Constant		0.5
Nozzle Cooling Air Wcl/W16		0.05

Table G3 (cont). Input Table for GASTURB Turbofan Modeling of Turbo-Ramjet

THIS PAGE IS INTENTIONALLY LEFT BLANK

LIST OF REFERENCES

1. Pratt, W.H., and Heiser, D.T., *Hypersonic Airbreathing Propulsion*, American Institute of Aeronautics and Astronautics, Inc., 1994.

2. Mondey, D., editor, "The International Encyclopedia of Aviation", Octopus Books, Ltd., 1977.

3. Rivera, G., *Turbochargers to Small Turbojet Engines for Uninhabited Aerial Vehicles*, Engineer's Thesis, Department of Aeronautics and Astronautics, U.S. Naval Postgraduate School, Monterey, CA, June 1998,

4. Hackaday, G., *Thrust Augmentation for a Small Turbojet Engine*, Master's Thesis, Department of Aeronautics and Astronautics, U.S. Naval Postgraduate School, Monterey, CA, March 1999.

5. Andreou, L., *Performance of a Ducted Micro-Turbojet Engine*, Master's Thesis, Department of Aeronautics and Astronautics, U.S. Naval Postgraduate School, Monterey, CA, September 1999.

6. Al-Namani, S. M., *Development of Shrouded Turbojet to Form a Turboramjet for Future Missile Applications*, Master's Thesis, Department of Physics, U.S. Naval Postgraduate School, Monterey, CA, June 2000.

7. Garcia, H., *Testing and Development of a Shrouded Gas Turbine Engine in a Freejet Facility*, Master's Thesis, Department of Physics, U.S. Naval Postgraduate School, Monterey, CA, December 2000.

8. Kurzke, J., *GASTURB 9.0 for Windows: A Program to Calculate Design and Off Design Performance of Gas Turbine Engines*, 2001.

9. Mattingly, J.D., Heiser, W.H., and Daley, D.H., *Aircraft Engine Design*, American Institute of Aeronautics and Astronautics, Inc., 1987.

10. Buning, P.G., Chiu, I.T., Obayashi, S., Rizk, Y.M., and Steger, J.L., "Numerical Simulation of the Integrated Space Shuttle Vehicle in Ascent", AIAA-88-4359-CP, AIAA Atmospheric Flight Mechanics Conference, Minneapolis, MN, August 1988.

11. Coyne, E., *Computational Analysis of the Off-design Performance of a Mach 6* $\left[\left(\frac{L}{D}\right)I_{sp}\right]_{\max}$ *Optimized Waverider*, Master's Thesis, Department of Aeronautics and Astronautics, U.S. Naval Postgraduate School, Monterey, CA, September 1999.

12. Williams, A.N., *Computational Fluid Dynamics Analysis of a Dual Mode Thruster*, Master's Thesis, Department of Aeronautics and Astronautics, U.S. Naval Postgraduate School, Monterrey, CA, September 1999.

INITIAL DISTRIBUTION LIST

1 Defense Technical Information center
Ft Belvoir, VA

2 Dudley Knox Library
Naval Postgraduate School
Monterey, CA

3 Prof Max Platzer
Chairman, Department of Aeronautics
Naval Postgraduate School
Monterey, CA

4 Prof Garth V. Hobson
Naval Postgraduate School
Monterey, CA

5 Prof Raymond P. Shreeve
Naval Postgraduate School
Monterey, CA

6 Naval Air Warfare Center Aircraft Division
Propulsion and Power Engineering
Patuxent River, MD
ATTN: C. Georgio, Code 4.4

7. Ross H. Piper III
Lakeside, CA